

Primordial power spectrum from the dressed metric approach in loop cosmologies

Bao-Fei Li^{1,2,3,*}, Parampreet Singh^{3,†} and Anzhong Wang^{2‡}

¹*Institute for Advanced Physics & Mathematics, Zhejiang University of Technology, Hangzhou, 310032, China*

²*GCAP-CASPER, Department of Physics, Baylor University, Waco, TX, 76798-7316, USA*

³*Department of Physics and Astronomy, & Center for Computation and Technology, Louisiana State University, Baton Rouge, LA 70803, USA*

We investigate the consequences of different regularizations and ambiguities in loop cosmological models on the predictions in the scalar and tensor primordial spectrum of the cosmic microwave background using the dressed metric approach. Three models, standard loop quantum cosmology (LQC), and two modified loop quantum cosmologies (mLQC-I and mLQC-II) arising from different regularizations of the Lorentzian term in the classical Hamiltonian constraint are explored for chaotic inflation in spatially-flat Friedmann-Lemaître-Robertson-Walker (FLRW) universe. In each model, two different treatments of the conjugate momentum of the scale factor are considered. The first one corresponds to the conventional treatment in dressed metric approach, and the second one is inspired from the hybrid approach which uses the effective Hamiltonian constraint. For these two choices, we find the power spectrum to be scale-invariant in the ultra-violet regime for all three models, but there is at least a 10% relative difference in amplitude in the infra-red and intermediate regimes. All three models result in significant differences in the latter regimes. In mLQC-I, the magnitude of the power spectrum in the infra-red regime is of the order of Planck scale irrespective of the ambiguity in conjugate momentum of the scale factor. The relative difference in the amplitude of the power spectrum between LQC and mLQC-II can be as large as 50% throughout the infra-red and intermediate regimes. Differences in amplitude due to regularizations and ambiguities turn out to be small in the ultra-violet regime.

I. INTRODUCTION

The inflationary paradigm not only resolves several long-standing puzzles in the standard cosmological model but also provides a framework to explain the formation of large scale cosmic structure in the universe [1, 2]. However, it also suffers from several problems, such as the origin of the inflaton field, the problem of the initial conditions and the past incompleteness of inflationary spacetimes due to big bang singularity. The conventional inflationary paradigm is essentially based on the classical description of spacetime dealing with physics at energy scales about $10^3 \sim 10^{12}$ orders of magnitude lower than the Planck scale [3, 4]. In order to resolve above open questions in the inflationary models, one has to turn to physics at the Planck scale which entails to understanding effects of the quantum description of spacetime. Any such quantum description is expected to involve quantization ambiguities. Under what conditions such ambiguities can reveal themselves in pre-inflationary physics is an interesting avenue to explore.

Loop quantum gravity (LQG) [5] is one of the leading approaches to quantize gravity whose avatar in symmetry reduced setting as loop quantum cosmology (LQC) has been extensively used to study cosmological implications of Planck scale physics [6]. A key prediction of LQC is that the big bang singularity is replaced by a quantum bounce due to the underlying discrete structure of

quantum geometry [7–10]. As a result, the evolution of the universe in LQC generically undergoes a contracting phase before the bounce followed by an expanding phase. At the fundamental level, the dynamics in LQC is dictated by a Hamiltonian constraint which is a second order quantum difference equation. For a large variety of physical states, quantum evolution can be very well approximated by an effective dynamics [11–13]. This effective dynamics has been shown to generically resolve all strong singularities [14] and lead to an interesting phenomenology [15]. Furthermore, the slow-roll inflationary phase can be naturally included in LQC and made past-complete using a minimally coupling of an inflaton to gravity [16–20]. After fixing the free parameters in the coupled system via the observed amplitude of the primordial scalar power spectrum and the scalar spectral index, the background dynamics from the bounce to the moment when the pivot mode exits the horizon can be completely fixed by the value of the scalar field and the sign of its velocity at the bounce. The nature of bounce and pre-inflationary dynamics is such that onset of inflation is natural to occur in LQC, even in the presence of anisotropies [21].

An important question is the way the pre-inflationary dynamics in loop cosmology results in signatures in the primordial power spectrum of the cosmological perturbations. Since LQC is a quantization of the homogeneous spacetimes and its connection with full LQG is not yet established, at present there are different approaches, based on different sets of assumptions, to understand quantum gravitational effects encoded in cosmological perturba-

* baofeili1@lsu.edu

† psingh@lsu.edu

‡ Anzhong.Wang@baylor.edu

tions. These approaches include¹: the deformed algebra approach [23–25], the dressed metric approach [26–28], the hybrid approach [29–31], and the separate universe approach [32]. Amongst these, the dressed metric and the hybrid approach have been extensively applied to phenomenology in recent times [28, 31, 33–43]. One common feature between these approaches is the usage of loop quantized background on which linear perturbations are treated using Fock quantization. In this paper, we focus on the dressed metric approach which uses elements from propagation of quantum test fields on quantum geometry [44]. In this approach, the quantum perturbations are described as propagating on a loop quantized background which can be effectively described by a dressed metric on a continuum spacetime with classical properties. For sharply peaked coherent states, evolution of the scale factor in the dressed metric is governed by the effective dynamics of LQC. The initial states for the perturbations are usually imposed right at the bounce as the obvious adiabatic states generated by an iterative process. Generally, the 4th-order adiabatic states are sufficient for the normalization of the energy momentum tensor of the perturbations [27]. Like hybrid approach, the dressed metric approach predicts an oscillating pattern of the power spectrum with amplified magnitude in a regime preceding the observed scale-invariant power spectrum in CMB. Since the comoving Hubble horizon is shrinking at the present time, these super-horizon modes with amplified magnitude can only be observed indirectly via the non-Gaussianity effects [40, 41].

While above developments provide novel ways to test features of quantum geometry as understood in LQC using CMB, we should note that there exist different regularizations of the Hamiltonian constraint and quantization ambiguities which can potentially affect physical implications. In LQC, one combines the Euclidean and Lorentzian parts of the Hamiltonian constraint using classical symmetries before quantization. If these parts are treated independently during quantization, one finds alternate in-equivalent quantizations of LQC. Two in-equivalent quantizations resulting in modified loop quantum cosmologies, mLQC-I and mLQC-II, were first studied by Yang, Ding and Ma [45]. Recently, mLQC-I was rediscovered by computing the expectation values of the Hamiltonian constraint using complexifier coherent states [46]. In mLQC-I one uses a classical identity on gravitational phase space to write the extrinsic curvature in the Lorentzian part of the Hamiltonian constraint in terms of holonomies. In contrast, in mLQC-II one uses symmetry between extrinsic curvature and Ashtekar-Barbero connection in the spatially-flat spacetime and then expresses the Lorentzian part in terms of holonomies. While, like LQC, mLQC-I and mLQC-II result in resolution of strong singularities [47], and genericness of inflation [4, 48], there are some striking

differences between these models. Unlike LQC where the quantum Hamiltonian constraint is a second order finite difference equation, in mLQC-I/II, the quantum Hamiltonian constraint is a fourth order quantum difference equation [49]. The effective Friedmann equations in mLQC-I/II contain higher than quadratic corrections in energy density [50]. The nature of bounce in mLQC-I is asymmetric [46] with an emergent Planck scale cosmological constant² [51], and a rescaled Newton’s constant in the contracting branch [50]. On the other hand, in mLQC-II, the background evolution is symmetric about the bounce as in LQC.

Apart from the various regularizations of the background Hamiltonians, there can also exist ambiguities related with the treatment of perturbations. The dressed metric approach is built on the classical perturbation theory in the Hamiltonian formalism [53]. This formalism converts the problem of solving a nonlinear partial differential equation (PDE) to the problem of solving one nonlinear ordinary differential equation (the background) and an infinite series of linear PDEs (the perturbations) [27]. The solutions of the lower order perturbations are required for solving the equations of motion of the higher order perturbations. As a result, in the equations of motion of the linear perturbations, there appears the conjugate momentum of the scale factor, namely π_a , of the background FLRW metric. The conjugate of the scale factor can be expressed in different ways. In the dressed metric approach this term has been treated conventionally using in part the classical Friedmann equation [28], whereas in the hybrid approach π_a is determined using effective Hamiltonian constraint. So far effects of these choices have not been compared, and it is pertinent to ask whether these ambiguities affect the primordial power spectrum. In the present work, we consider two choices of π_a for each model. The first choice uses the conventional treatment in dressed metric approach, and the second choice is based on the treatment in hybrid approach and generalized appropriately to mLQC-I and mLQC-II. It turns out that conventional treatment of momentum of scale factor in dressed metric also results in a subtlety with a potential term in equation of motion of perturbations. Effects of this subtlety become transparent if initial conditions are imposed before the bounce. In such a case, there is a discontinuity in potential term which in particular results in drastic effects in the UV regime of power spectrum for mLQC-I, essentially ruling out the model. We show that this problem can be resolved by considering a smooth function interpolating the potential term before and after the bounce.

² Interestingly the nature of matter in pre-bounce regime is determined by the way areas of loops, over which holonomies are considered, is assigned. If instead of ‘improved dynamics’ or $\bar{\mu}$ -scheme [9] as used in the manuscript, one uses μ_0 -scheme of LQC [8], one obtains an emergent matter with equation of state of a string gas or an effective negative spatial curvature term [52].

¹ See [22] for earlier works preceding these approaches.

The goal of this manuscript is to compare primordial power spectrum of cosmological perturbations for LQC, mQLC-I and mLQC-II using the dressed metric approach. Previous works have investigated properties of power spectrum in LQC [26–28, 33, 35] as well as mLQC-I [54]. Our objective is to not only compare predictions from different regularizations but also understand effects due to different choices of π_a . Unlike the conventional approach where initial conditions are set at the bounce, we consider initial conditions in the contracting branch and point out certain subtleties in the process. Choosing initial conditions in the contracting branch allows us to test the robustness of results on primordial perturbations in LQC. Further, given that in mLQC-I dynamics in the pre-bounce phase is significantly different from the post-bounce phase, the primordial power spectrum is sensitive to whether we choose the initial conditions for perturbations at the bounce or in the pre-bounce regime. For the latter, where one can use the Bunch-Davies (BD) vacuum initial conditions for mLQC-I, we find a Planckian scale amplitude of the power spectrum in the infra-red (IR) regime. This turns out to be the main discriminating feature between mLQC-I and the other two models.

Our analysis is performed using the chaotic ϕ^2 potential. Although it is constrained by CMB observations due to its large tensor-to-scalar ratio, it essentially possesses the same qualitative properties as of more favored potentials, like the Starobinsky potential. Note that if the bounce is dominated by the kinetic energy of the inflaton, as is generally considered in previous studies, the form of inflationary potentials play a little role in the pre-inflationary regime where quantum gravity effects are most important [16–20]. As a result, many features of LQC as studied for CMB [28, 31, 33–43] are at least qualitatively independent of the choice of potential. Thus, even though one can use more favorable potentials such as the Starobinsky potential and the monodromy potential, we do not expect any qualitative differences to results from our analysis, especially the ones resulting from physics of the bounce regime. This allows a direct and transparent comparison with phenomenological implications from primordial power spectrum using dressed metric approach studied in detail using ϕ^2 potential for LQC in Ref. [28], permitting us to focus on differences resulting from ambiguities in comparison to earlier works.

For the background dynamics in LQC, we use the same initial conditions as in [28]. While, for the other models, like mLQC-I and mLQC-II, we carefully choose the initial conditions so that the inflationary e-folds are exactly same in all three models. To be more specific, the number of the inflationary e-foldings in all three models is set to 72.8 to ensure that quantum gravity effects are possibly observable in the CMB. Under these conditions, we find that differences between these models and results from ambiguities in π_a do not affect the UV part of the power spectrum. But there are significant differences in the IR and the oscillatory regime. The relative difference in magnitude of power spectrum can be at least

10% in the latter regimes purely from the ambiguity in π_a . Differences between LQC and mLQC-II can be as large as 50% in these regimes. There are huge differences between mLQC-I and other two models in the IR regime with power spectrum in mLQC-I having an extremely large magnitude due to Planck sized emergent cosmological constant in the contracting branch.

This paper is organized as follows. In Sec. II, we begin with a brief summary of the first-order perturbation theory and dressed metric approach in LQC, and then we continue to fix the free parameters in the slow-roll inflationary model and the adiabatic initial states of the perturbations. Finally, we present and compare the scalar power spectrum in LQC with two different regularizations of π_a . In Sec. III, the scalar power spectrum in mLQC-I is obtained on the same lines as in Sec. II, and the emphasis is placed on the peculiarities of contracting phase of the model. In Sec. IV, the power spectrum in mLQC-II is presented and compared with LQC. Also the tensor perturbations in all three models are discussed and compared. We summarize our main results in Sec. V. In the appendix, we discuss the consequence of a discontinuity at the bounce in the equations of motion of the perturbations in each model. Our analysis in this paper will be based on assuming validity of all assumptions underlying the dressed metric approach and that the approach can be extended to mLQC-I and mLQC-II. Throughout this paper, we use $c = G = \hbar = 1$.

II. BASICS OF DRESSED METRIC APPROACH IN LQC

This section is divided into three parts. In the first part, a brief review of the dressed metric approach in LQC is given and a special emphasis is put on the different ways to deal with the conjugate momentum of the scale factor in the equations of motion of the linear perturbations. In the second part, after fixing the parameters in the slow-roll model, the initial conditions of both background dynamics and the perturbations are discussed. Finally, numerical simulations of the primordial power spectrum are presented. As both the approach and the results have already be extensively studied in the literature, only the most necessary parts that are relevant to our discussion are recalled. For more detailed exposition of this approach and its implications, one can refer to seminal papers [26–28].

A. The dressed metric approach in LQC

1. Brief review of the perturbation theory in the Hamiltonian formalism

In the dressed metric approach, the quantum fluctuations are described as propagating on a quantum background spacetime which can be described by a dressed

metric. The general formalism is based on the Hamiltonian formulation of the perturbation theory in general relativity introduced by Langlois [53]. In the following, we consider a single scalar field minimally coupled to gravity on a spatially-flat FLRW background. Therefore, the phase space consists of fields: $\Gamma = \{\Phi, \pi_\Phi, h_{ij}, \pi^{ij}\}$, which is endowed with the canonical Poisson brackets:

$$\begin{aligned} \{\Phi(x), \pi_\Phi(y)\} &= \delta^3(x-y), \\ \{h_{ij}(x), \pi^{kl}(y)\} &= \frac{1}{2} (\delta_i^k \delta_j^l + \delta_i^l \delta_j^k) \delta^3(x-y). \end{aligned} \quad (2.1)$$

The Hamiltonian function of this coupled system takes the form [53]

$$H = \int d^3x (N\mathcal{H} + N^i\mathcal{H}_i), \quad (2.2)$$

where

$$\begin{aligned} \mathcal{H} &= \frac{2\kappa}{\sqrt{h}} \left(\pi^{ij}\pi_{ij} - \frac{\pi^2}{2} \right) - \frac{\sqrt{h}}{2\kappa} R + \frac{\pi_\Phi^2}{2\sqrt{h}} \\ &\quad + \sqrt{h}V + \frac{\sqrt{h}}{2} \partial_i \phi \partial^i \phi, \end{aligned} \quad (2.3)$$

$$\mathcal{H}_i = -2\partial_k (h_{ij}\pi^{jk}) + \pi^{lm}\partial_i h_{lm} + \pi_\Phi \partial_i \phi. \quad (2.4)$$

Here $\kappa = 8\pi G$, h is the determinant of the three-metric, R denotes the intrinsic Ricci scalar on the three-surface, and V is the self-interaction potential term of the scalar field. The perturbations around the background can be written in the following form:³

$$\begin{aligned} \Phi &= \phi(t) + \delta\phi(t, x), \\ \pi_\Phi &= p_\phi(t) + \delta p_\phi(t, x), \\ h_{ij} &= \hat{h}_{ij}(t) + \delta h_{ij}(t, x), \\ \pi^{ij} &= \hat{\pi}^{ij}(t) + \delta\pi^{ij}(t, x), \end{aligned} \quad (2.5)$$

Here $\Gamma_0 = \{\phi(t), p_\phi(t), \hat{h}_{ij}(t), \hat{\pi}^{ij}(t)\}$ is the phase space of the spatially-flat FLRW background and the phase space of the perturbations $\Gamma_1 = \{\delta\phi(t, x), \delta p_\phi(t, x), \delta h_{ij}(t, x), \delta\pi^{ij}(t, x)\}$ are regarded as purely inhomogeneous. In the following, the arguments of both background and perturbations are suppressed for simplicity.

³ Note that in this approach of Hamiltonian theory of perturbations, the lapse and shift functions are regarded as Lagrange multipliers and hence no perturbations of these two functions are considered. The method is restrictive in being unable to provide a natural canonical description in terms of gauge-invariant variables except Mukhanov-Sasaki variables, such as the Bardeen potentials whose natural interpretation is tied to longitudinal gauge requiring fixing perturbation in the shift variable. However, this formalism can be generalized to bring it closer to covariant approach and to investigate canonical formalism in terms of all gauge-invariant variables, not only the Mukhanov-Sasaki variables, by treating the lapse and shift functions as the dynamical variables in an extended phase space [57].

The dynamics in the perturbation theory is determined order by order, with Eq. (2.5) plugged into Eq. (2.3)-(2.4) and then truncating the result at the required order. If the linear order perturbations are considered, one should keep the terms up to the second order in the perturbations. In the following, we briefly summarize the results until the second order (for details see [41, 53]).

Zerth order: As the spatially-flat FLRW background is both homogeneous and isotropic, the phase space Γ_0 is four dimensional, composed of $\{a, \pi_a, \phi, p_\phi\}$. The scale factor a and its conjugate momentum π_a are related with \hat{h}_{ij} and $\hat{\pi}^{ij}$ via

$$\hat{h}_{ij} = a^2 \delta_{ij}, \quad \hat{\pi}^{ij} = \frac{\pi_a}{6a} \delta^{ij}, \quad (2.6)$$

which, once plugged back into Eqs. (2.3)-(2.4), give scalar and vector constraints at the zeroth order, that is

$$\mathcal{H}^{(0)} = -\frac{\kappa\pi_a^2}{12a} + \frac{p_\phi^2}{2a^3} + a^3V \approx 0, \quad (2.7)$$

and $\mathcal{H}_i^{(0)}$ vanishes identically. $\mathcal{H}^{(0)}$ is the classical background Hamiltonian constraint whose vanishing yields the classical Friedmann equation in spatially-flat FLRW cosmology. The zeroth order Hamiltonian is a direct result of Eqs. (2.2) and (2.7) with only one subtlety. Since the spatial manifold is noncompact, any integral of homogenous fields would inevitably become infinite. In order to avoid such spurious divergences, one can simply restrict the integrals to the fiducial cell with comoving volume \mathcal{V}_o . In this way, the Hamiltonian at zeroth order reads

$$\mathcal{H}_0 = N(t)\mathcal{V}_o\mathcal{H}^{(0)}, \quad (2.8)$$

with the only nonvanishing Poisson bracket being $\{a, \pi_a\} = \{\phi, p_\phi\} = 1/\mathcal{V}_o$. The dynamics of the background is thus prescribed by the Hamilton's equations for the phase space variables (a, π_a, ϕ, p_ϕ) . In particular, the equation of motion of the scale factor is given by

$$\dot{a} = -N \frac{\kappa\pi_a}{6a}, \quad (2.9)$$

which in turn relates the momentum π_a with the Hubble rate H via

$$\pi_a = -6Ha^2/(N\kappa). \quad (2.10)$$

It is worth noting that the Hamilton's equations do not depend on \mathcal{V}_o which is an infrared regulator with no physical significance.

First order: The first-order scalar and vector constraints can be computed in a straightforward way from Eqs. (2.3)-(2.4). As is well-known, any 3×3 symmetric tensor can be decomposed into two scalar components, two vector components and two tensor components. The

first-order scalar and vector constraints turn out to be equivalent to two constraints on the scalar components and two constraints on the vector components. Thus, there is only one degree of freedom (DOF) in the scalar sector which corresponds to the comoving curvature perturbation \mathcal{R} and two DOFs in the tensor sector which are two transverse and traceless primordial gravitational wave polarizations. The vector sector has no physical DOF unless other vector field perturbations are introduced into the system.

Since the primordial power spectrum is computed in the momentum space, in the following, we only deal with the linear perturbations in the momentum space which are

$$\delta\tilde{h}_{ij}(\vec{k}) = \int \frac{d^3x}{(2\pi)^3} \delta h_{ij}(\vec{x}) e^{-i\vec{k}\cdot\vec{x}}.$$

Hereafter, both the tilde and the argument of $\tilde{h}_{ij}(\vec{k})$ are suppressed for simplicity. In order to extract scalar/vector/tensor components of δh_{ij} and $\delta\pi^{ij}$, one can introduce a set of orthogonal basis A_{ij}^m , where $m = 1, 2, \dots, 6$ and then project δh_{ij} onto it as

$$\delta h_{ij} = \gamma_m A_{ij}^m. \quad (2.11)$$

Here γ_1 and γ_2 are the scalar components when the first two A_{ij}^m are given by

$$A_{ij}^1 = \hat{h}_{ij}, \quad A_{ij}^2 = \hat{k}_i \hat{k}_j - \frac{1}{3} \hat{h}_{ij}. \quad (2.12)$$

Meanwhile, the conjugate momentum of γ_m can be derived from $\pi^{(m)} = A_{ij}^m \delta\pi^{ij}$. In terms of the scalar components $\gamma_1, \gamma_2, \delta\phi$ and their conjugate momenta, the scalar constraint at the linear order takes the form [53]

$$E = -\frac{\kappa\pi_a^2\gamma_1}{24a} - \frac{3p_\phi^2\gamma_1}{4a^3} + \frac{3\gamma_1 a^3 V}{2} - \frac{ak^2\gamma_1}{\kappa} + \frac{ak^2\gamma_2}{3\kappa} - \frac{\kappa\pi_a\pi^{(1)}}{3a^2} + \frac{p_\phi\delta p_\phi}{a^3} + a^3 V_{,\phi}\delta\phi, \quad (2.13)$$

while the projection of the vector constraint onto the scalar modes reads

$$M = \frac{a}{6}\pi_a\gamma_1 - \frac{2a}{9}\pi_a\gamma_2 - \frac{2}{3}\pi^{(1)} - 2\pi^{(2)} + p_\phi\delta\phi. \quad (2.14)$$

It can be easily checked that both E and M commute with themselves and they also commute with each other due to the classical background Hamiltonian constraint Eq. (2.7).

Second order: The dynamics of the scalar and tensor modes in the linear perturbations is prescribed by the Hamiltonian at the second order in the linear perturbations. For the scalar part, due to the two first-class constraints E and M , it's necessary to first separate the gauge DOFs from the true physical DOFs in the scalar subspace spanned by $\{\gamma_1, \gamma_2, \delta\phi\}$ and their conjugate momenta. One can do this in two steps:

1. Rewrite two constraints in their equivalent forms:

$$E = \pi^{(1)} - f_1(\gamma_1, \gamma_2, \delta\phi, \delta p_\phi) \equiv P_1^*, \\ M = \pi^{(2)} - f_2(\gamma_1, \gamma_2, \delta\phi, \delta p_\phi) \equiv P_2^*. \quad (2.15)$$

Thus, we can safely choose $\{\gamma_1, P_1^*, \gamma_2, P_2^*\}$ as the canonical variables for gauge DOFs. On the other hand, following Langlois's approach [53], the canonical pair for the physical sector can be chosen as the Mukhanov-Sasaki's variable Q and its conjugate momentum P .

2. Solving for the generating function S of the canonical transformation from the constraints E and M by replacing the canonical momenta in these constraints by the partial derivatives of the generating function with respect to their respective canonical variables, the resulting Hamiltonian for the physical sector can be shown as [53]

$$H_S = \frac{N(t)}{2} \int d^3k \left(\frac{P_s^2}{a^3} + a(\Omega_Q^2 + k^2) Q_s^2 \right), \quad (2.16)$$

where

$$\Omega_Q^2 = 3\kappa \frac{p_\phi^2}{a^4} - 18 \frac{p_\phi^4}{a^6 \pi_a^2} - 12a \frac{p_\phi}{\pi_a} V_{,\phi} + a^2 V_{,\phi\phi}. \quad (2.17)$$

Above $V_{,\phi}$ denotes the derivative of the potential with respect to the scalar field ϕ . On the other hand, there exists no constraints on the tensor modes and their Hamiltonian is given by

$$H_T = N(t) \int d^3k \left(2\kappa \frac{P_t^2}{a^3} + \frac{a}{8\kappa} k^2 Q_t^2 \right). \quad (2.18)$$

Thus, the dynamics of the scalar and tensor perturbations denoted collectively by \mathcal{Q} are prescribed by the Hamilton's equations $\dot{\mathcal{Q}} = \{Q, H_Q\}$, where $H_Q = H_S$ or H_T given respectively by Eq. (2.16) for scalar, or (2.18) for tensor perturbations. The tensor modes can also be regarded as two massless scalar modes, as H_S in Eq. (2.16) reduces to H_T in Eq. (2.18) when the potential term (and thus Ω^2) vanishes and meanwhile setting

$$Q_t = \sqrt{32\pi G} Q_s, \quad P_t = \frac{P_s}{\sqrt{32\pi G}}. \quad (2.19)$$

Therefore, in the following, we mainly focus on the scalar modes, knowing that the tensor modes can be recovered by setting $V = 0$ and the normalization condition Eq. (2.19).

2. The dressed metric approach

Now that the classical physical degrees of freedom and their Hamiltonians are known, we can proceed with the quantization of the classical perturbation theory. The classical phase space consists of the homogeneous sector and the inhomogeneous perturbations. Similarly, in the quantum theory, the quantum state is assumed to be a

tensor product of the homogeneous and inhomogeneous quantum states as

$$|\psi\rangle = |\psi_0\rangle \times |\psi_1\rangle, \quad (2.20)$$

where $|\psi_0\rangle$ stands for the quantum background while $|\psi_1\rangle$ is the quantized inhomogeneous perturbations. The background is quantized using the polymer quantization as in LQC [7, 9], and the resulting quantum equation of motion for the quantum state ψ_0 is a difference equation which reads [7]

$$-i\hbar\partial_\phi\psi_0(\tilde{\nu}, \phi) = \hat{H}_0\psi_0(\tilde{\nu}, \phi), \quad (2.21)$$

with $\hat{H}_0 = \hbar\sqrt{\Theta}$ and

$$\Theta\psi_0(\tilde{\nu}, \phi) = \frac{3\pi G}{\lambda^2}\tilde{\nu}\left\{(\tilde{\nu} + 2\lambda)\psi_0(\tilde{\nu} + 4\lambda, \phi) - 2\tilde{\nu}\psi_0(\tilde{\nu}, \phi) + (\tilde{\nu} - 2\lambda)\psi_0(\tilde{\nu} - 4\lambda, \phi)\right\}, \quad (2.22)$$

where $\tilde{\nu} = a^3/(2\pi G\gamma)$, $\lambda^2 = 4\sqrt{3}\pi\gamma l_{\text{Pl}}^2$ is the smallest nonzero eigenvalue of the area operator and γ is the Barbero-Immirzi parameter. In LQC, the value of Barbero-Immirzi parameter is fixed to $\gamma \approx 0.2375$ using black hole thermodynamics in LQG. Note that the above Schrödinger-like equation is only valid for the massless scalar field. In principle, one can add a potential term with a subtlety that ϕ does no longer serve as a good clock, especially in the reheating phase. Further, the effective Hamiltonian and modified Friedmann equations used in LQC have been so far derived only for the massless scalar field case. As in previous works, we assume the validity of effective equations when a non-vanishing potential is present. This assumption gets support from numerical simulations with potentials where effective dynamics is found to be in excellent agreement with quantum evolution [55].

In the dressed metric approach, the inhomogeneous perturbations, Fock quantized, can be interpreted as propagating on a quantum background spacetime with the effective metric given by

$$\tilde{g}_{ab}dx^a dx^b = \tilde{a}(-d\tilde{\eta}^2 + dx_i dx^i), \quad (2.23)$$

where

$$\tilde{a}^4 = \frac{\langle \hat{H}_0^{-1/2} \hat{a}^4 \hat{H}_0^{-1/2} \rangle}{\langle \hat{H}_0^{-1} \rangle}, \quad (2.24)$$

$$d\tilde{\eta} = \left(\langle \hat{H}_0^{-1} \rangle \langle \hat{H}_0^{-1/2} \hat{a}^4 \hat{H}_0^{-1/2} \rangle \right)^{1/2} d\phi. \quad (2.25)$$

The expectation values in the above formula are evaluated with respect to the background state ψ_0 . The equations of motion of the perturbations take the same form as in the classical perturbation theory which can be formally derived from Eq. (2.16) as

$$\ddot{Q}_k + 3H\dot{Q}_k + \frac{k^2 + \tilde{\Omega}^2}{\tilde{a}^2}Q_k = 0, \quad (2.26)$$

where $H = \dot{\tilde{a}}/\tilde{a}$. The expression for $\tilde{\Omega}^2$ is given by

$$\tilde{\Omega}^2 = \frac{\langle \hat{H}_0^{-1/2} \hat{a}^2 \hat{\Omega}^2 \hat{a}^2 \hat{H}_0^{-1/2} \rangle}{\langle \hat{H}_0^{-1/2} \hat{a}^4 \hat{H}_0^{-1/2} \rangle}, \quad (2.27)$$

here $\hat{\Omega}^2$ is the quantum operator of Ω_Q^2 in Eq. (2.17). In the actual numerical simulations of the power spectrum, we usually employ the test-field approximation in which the background state ψ_0 is chosen to be highly peaked around its classical trajectories during the inflationary region⁴, thus all the background quantities in Eq. (2.26) can be replaced by those from the effective theory of LQC in which the effective dynamics is determined by the Hamiltonian constraint

$$\mathcal{H}_0^{\text{LQC}} = -\frac{3v \sin^2(\lambda b)}{8\pi G\lambda^2\gamma^2} + \frac{p_\phi^2}{2v} + vV(\phi) \approx 0, \quad (2.28)$$

where $v = a^3$ and the Poisson brackets are given by $\{b, v\} = 4\pi G\gamma$ and $\{\phi, p_\phi\} = 1$. Therefore, the equations of motion in the effective theory take the form

$$\dot{v} = \frac{3v}{2\lambda\gamma} \sin(2\lambda b), \quad (2.29)$$

$$\dot{b} = -\frac{3 \sin^2(\lambda b)}{2\gamma\lambda^2} - 4\pi G\gamma \left(\frac{p_\phi^2}{2v^2} - V \right), \quad (2.30)$$

$$\dot{\phi} = \frac{p_\phi}{v}, \quad \dot{p}_\phi = -vV_{,\phi}. \quad (2.31)$$

The bounce in LQC takes place when the energy density of the scalar field reaches the critical energy density $\rho_c = 3/(8\pi G\gamma^2\lambda^2)$. It should be noted that in order to apply the effective Hamilton's equations to the background quantities in Eq. (2.17), one has to be careful with the $1/\pi_a$ factor as there is ambiguity in dealing with it at the level of effective theory. If the classical equation of π_a in Eq. (2.10) is directly substituted into Eq. (2.17), Ω_Q^2 is singular right at the bounce where the Hubble rate and π_a vanish. In order to avoid this singularity, in [27, 28], the zeroth order classical constraint in Eq. (2.7) is used to replace $1/\pi_a^2$ by $\kappa/(12a^4\rho)$, where ρ is the energy density of the scalar field. This leads to an expression of Ω_Q^2 in terms of the potential and its derivatives, using the classical Hamiltonian constraint, which reads⁵

$$\Omega_\pm^2 = a^2 (V_{,\phi\phi} \pm 2fV_{,\phi} + f^2V), \quad (2.32)$$

with $f = \sqrt{24\pi G/\rho}\dot{\phi}$. Here, for brevity we have suppressed the subscript Q in Ω_\pm^2 . Note Ω_\pm^2 vanishes identically for the tensor modes. In Eq. (2.32), the subscript

⁴ Our analysis will assume the validity of this approximation in all the considered models. In particular, we assume that subtleties noted in Ref. [56] can be addressed using sharply peaked states.

⁵ Note the second term in the parenthesis of Eq. (2.32) is different from Eq. (A8) in [28]. We follow the expression given by Eq. (4.7) in [39]. See also [42].

‘ \pm ’ indicates the sign in front of the term $2fV_{,\phi}$. Moreover, Ω_+ is valid only in the expanding phase where π_a is negative, while Ω_- is valid in the contracting phase where π_a becomes positive. If the initial conditions for perturbations are given right at the bounce, then Ω_+ suffices. But, if one is interested in exploring the evolution of perturbation through the bounce, then one needs a corresponding equation for the contracting phase with Ω_-^2 and match the potentials Ω_{\pm}^2 at the bounce. As we would see in the following, Ω_+^2 and Ω_-^2 do not coincide at the bounce, because of the behavior of π_a across the bounce, and one needs a smooth interpolation to propagate perturbations across the bounce.

In Sec. III and IV, the dressed metric approach is applied to two other loop cosmological models, i.e. mLQC-I and mLQC-II. The difference among these three models lies only in the regularization of the homogeneous sector, as a result the Schrödinger’s equation of the background state ψ_0 is modified. The form of the equation of motion of the linear perturbations remain unchanged since the classical second-order Hamiltonian is not changed and the same Fock representation is used to quantize these perturbations. As a result, Eq. (2.26) is still valid in both mLQC-I and mLQC-II, and the only difference comes from the background dynamics which should be prescribed by the effective Hamiltonian in each case.

B. Fixing the parameters in the slow-roll model and the initial conditions for the numeric simulations

In order to compare our results with those in the dressed metric literature, we use the WMAP data [58] in which the pivot mode $k_0^* = 0.002 \text{ Mpc}^{-1}$. From the observed scalar power spectrum $A_s = 2.43 \times 10^{-9}$ and the scalar spectral index $n_s = 0.968$ with error bars of about $\pm 4.50\%$ for A_s and $\pm 1.25\%$ for n_s , the relevant parameters in the slow-roll inflationary model with $V = \frac{1}{2}m^2\phi^2$, can be uniquely fixed as [17]:

$$\begin{aligned} m &= 1.21 \times 10^{-6}, & \phi_* &= \pm 3.15, \\ H_* &= 7.83 \times 10^{-6}, & \phi_e &= 0.282, \end{aligned} \quad (2.33)$$

where the star denotes the quantities at the moment when the pivot mode exits the horizon in the slow-roll inflation, and ϕ_e is the value of the scalar field at the end of the inflation. From these quantities, one can first fix the e-folds from the horizon exit to the end of inflation which can be shown as

$$N_* = \int_{\phi_{\text{end}}}^{\phi_*} d\phi \frac{8\pi V}{V_{,\phi}} = 61.8. \quad (2.34)$$

On the other hand, the comoving wavenumber of the pivot mode can be simply computed as

$$k_* = a_* H_* = a_0 k_0^*, \quad (2.35)$$

where k_0^* is the pivot mode observed today, namely $k_0^* = 0.002 \text{ Mpc}^{-1}$, and a_0 is the scale factor at present.

Thus the e-folds from the horizon crossing to the present is about 126. This indicates that if the initial conditions in LQC are imposed at the bounce, they would only affect the background dynamics from the bounce to the horizon crossing since the LQC corrections to general relativity are negligible in the slow-roll phase, considering the energy scale of the slow-roll is about 10^{-12} order of magnitude lower than the Planck scale.

Our numeric simulations are based on the Hamilton’s equations (2.29)-(2.31). If the initial conditions of the background are imposed right at the bounce, then the only free parameter is the value of the scalar field ϕ_B (also the sign of $\dot{\phi}_B$ is left undetermined). The other parameters can be fixed as $v_B = 1$, $b_B = \frac{\pi}{2\lambda}$ and the magnitude of p_ϕ is determined by the identity $\rho_c = \frac{1}{2}p_\phi^2 + \frac{1}{2}m^2\phi_B^2$ at the bounce. In our numeric simulations, the cosmic time t is set to zero at the bounce. We first choose some ϕ_B at the bounce then evolve the universe backwards in time until $t = t_p < 0$. Then at $t = t_p$, the initial conditions for the linear perturbations are chosen to be the adiabatic states which are the solutions of the equation

$$\nu_k'' + (k^2 + s)\nu_k = 0, \quad (2.36)$$

where $\nu_k = aQ_k$ and s is the effective mass squared term in the model. The general WKB solution of the above equation can be written in the form

$$\nu_k = \frac{1}{\sqrt{2W_k}} e^{-i \int^\eta W_k(\bar{\eta}) d\bar{\eta}}, \quad (2.37)$$

which, once plugged back into Eq. (2.36), generates a differential equation of W_k that takes the form

$$W_k^2 = k^2 + s - \frac{W_k''}{2W_k} + \frac{3}{4} \left(\frac{W_k'}{W_k} \right)^2. \quad (2.38)$$

Now, the n th-order adiabatic state can be derived by plugging into the right hand side of Eq. (2.38) the $(n-2)$ th order solution. If we take the Minkowski vacuum as the zeroth order solution, namely $W_k^{(0)} = k$, the second order adiabatic solution can be easily found as

$$W_k^{(2)} = \sqrt{k^2 + s}. \quad (2.39)$$

Thus, the second order obvious adiabatic state considered in [28] is obtained by performing an asymptotic expansion of the solution (2.39) in the limit of large k and then truncating it to the second order. This procedure can be continued to an arbitrary order. However, for our purposes, it is sufficient to consider the fourth order adiabatic state, which is explicitly given by

$$W_k^{(4)} = k + \frac{s}{2k} - \frac{s^2 + s''}{8k^3}. \quad (2.40)$$

In our simulations, this initial state of the linear perturbations is imposed at some finite time in the contracting phase where $W_k^{(4)}$ is positive for all the modes $k \geq 10^{-6}$.

Although the mass squared term s depends on the model and the potential, one can choose a time far before the bounce so that $W_k^{(4)}$ is positive for Ω^2 and Ω_{eff}^2 in both LQC and mLQC-II when $k \geq 10^{-6}$. Our choice of this initial time is $t/t_{\text{Pl}} = -1.10 \times 10^5$. The results are robust for different choices of the initial time as long as it is chosen such that $W_k^{(4)} > 0$ for relevant modes.

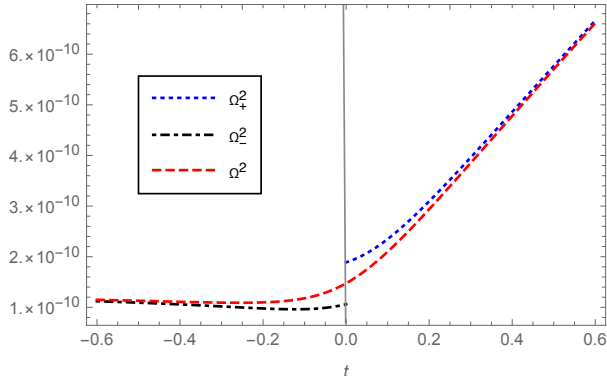


FIG. 1. This figure shows the difference between Ω_+^2 , Ω_-^2 and Ω^2 near the bounce in the cosmic time for LQC. The blue dotted line represents Ω_+^2 in the expanding phase, the black dot-dashed line is for Ω_-^2 in the contracting phase while the red dashed line is the smooth extension Ω^2 which connects Ω_+^2 with Ω_-^2 near the bounce. The middle vertical gray line represents the bounce point at $t = 0$.

C. The primordial power spectrum

One of the most important features of the primordial power spectrum is that the magnitude of the comoving curvature perturbations freezes once these modes exit the Hubble horizon in the inflationary epoch. The primordial power spectrum $P_{\mathcal{R}}$ is usually evaluated at the end of inflation by

$$P_{\mathcal{R}} = \frac{k^3}{2\pi^2} \frac{|Q_k|^2}{z^2}, \quad (2.41)$$

where $z = \dot{\phi}/H$ and Q_k is computed from Eq. (2.26) with the normalization condition

$$Q_k \dot{Q}_k^* - Q_k^* \dot{Q}_k = \frac{i}{a^3}, \quad (2.42)$$

where the star denotes the complex conjugate and a dot stands for a derivative with respect to the cosmic time. Similarly, the primordial power spectrum of the tensor perturbations is given by

$$P_{\mathcal{T}} = \frac{16k^3}{\pi} |Q_k|^2, \quad (2.43)$$

with the same normalization condition Eq. (2.42). The initial conditions for the background are chosen at the

bounce (we first try $\phi_B = 1.15 m_{\text{Pl}}$ and $\dot{\phi}_B > 0$ in order to compare our results with those in [28]), then the universe is first evolved backwards in time until $t_p = -1.10 \times 10^5 t_{\text{Pl}}$ in the contracting phase where the initial conditions of the linear perturbations are imposed. With $\phi_B = 1.15 m_{\text{Pl}}$ at the bounce, the number of e-folds from the bounce to the onset of the slow-roll is 4.21 and the inflationary e-folds are 72.8. The initial states of the scalar perturbations are the adiabatic states introduced in the last subsection. In particular, for the scalar perturbations, the mass squared term s in Eqs. (2.39)-(2.40) is explicitly given by

$$s = \Omega_o^2 - \frac{a''}{a}. \quad (2.44)$$

Here a''/a (in the spatially-flat FLRW spacetime, the Ricci scalar $R = 6a''/a^3$) is the curvature term determined by the geometry of the background spacetime while Ω_o^2 denotes the corresponding expression for any given model, including Ω_Q^2 , Ω_{\pm}^2 , or Ω^2 introduced below. In all cases it is determined by the potential of the scalar field, and can be regarded as an effective potential term for the perturbations in the considered background spacetime. In terms of the variables Q_k and its derivative, the initial conditions are equivalent to

$$Q_k = \frac{1}{a(t_p) \sqrt{2W^{(n)}(t_p)}},$$

$$\dot{Q}_k = \frac{dQ_k}{dt} \Big|_{t=t_p} - \frac{i}{a^2(t_p)} \sqrt{\frac{W^{(n)}(t_p)}{2}}, \quad (2.45)$$

where $W^{(n)}$ denotes the n th adiabatic state, in particular, $W^{(0)} = k$ is the Minkowski vacuum.

Before proceeding to the main results on the power spectrum, we would like to clarify the Ω_Q^2 term employed in our simulations. Basically, there are two ansatz for Ω_Q^2 . One is by using the classical Friedmann constraint as discussed in Sec. II.A, which leads to Ω_{\pm}^2 in Eq. (2.32). However, as Ω_+^2 and Ω_-^2 do not coincide at the bounce, the second ansatz is a smooth extension which connects Ω_+^2 in the expanding phase with Ω_-^2 in the contracting phase is required. Inspired by the hybrid approach (see Eq. (2.48)), this smooth extension can be given by

$$\Omega^2 = a^2 (V_{,\phi\phi} + 2 \cos(\lambda b) f V_{,\phi} + f^2 V). \quad (2.46)$$

The difference between Ω_+^2 , Ω_-^2 and Ω^2 near the bounce are compared in Fig. 1. Since $\cos(\lambda b)$ behaves like a step function across the bounce, Ω^2 quickly tends to Ω_+^2 in the expanding phase, and to Ω_-^2 in the contracting phase. Moreover, it takes the average value of Ω_+^2 and Ω_-^2 at the bounce. In the appendix, we compare the power spectrum resulting from Ω^2 with Ω_{\pm}^2 , and show that differences are rather small for LQC as well as mLQC-II. However, for mLQC-I there is a significant difference with a divergent power spectrum in UV regime if Ω_{\pm}^2 is used. The second ansatz to incorporate $1/\pi_a$ and $1/\pi_a^2$ terms is

motivated from the hybrid approach in which these terms are effectively given by [29, 30]

$$\frac{1}{\pi_a^2} \rightarrow \frac{16\pi^2 G^2 \gamma^2 \lambda^2}{9a^4 \sin^2(\lambda b)}, \quad (2.47)$$

$$\frac{1}{\pi_a} \rightarrow \frac{-4\pi\gamma\lambda \cos(\lambda b)}{3a^2 \sin(\lambda b)}. \quad (2.48)$$

Note if Eq. (2.47) is used in the classical background Hamiltonian constraint, one directly arrives at the effective Hamiltonian constraint in LQC given by Eq. (2.28). Besides, the $\cos(\lambda b)$ term in Eq. (2.48) makes $1/\pi_a$ smooth near the bounce and meanwhile picks up the same sign of π_a as in the classical case in both contracting and expanding phases. In the following, we call Ω^2 derived from the substitutions Eqs. (2.47)-(2.48) as Ω_{eff}^2 . However, it is important to note that the replacement in Eq. (2.47) is only valid in the effective dynamics of LQC, and not for mLQC-I and mLQC-II. For latter models, a similar substitution can be made using the same motivation.

In order to compare two different ansatz, it is necessary to understand the way Ω^2 and Ω_{eff}^2 would change in the entire range from the moment where the initial conditions of the perturbations are imposed to the time when the power spectra are evaluated. Fig. 2 is plotted for this purpose. In the first panel, Ω^2 , Ω_{eff}^2 and a''/a are compared in the interval $t/t_{\text{Pl}} \in (0, 2 \times 10^4)$. It can be seen from this figure that the difference between Ω^2 and Ω_{eff}^2 becomes negligible after $t/t_{\text{Pl}} = 1000$ while for $t/t_{\text{Pl}} \in (0, 5000)$, the curvature term is much larger than the potential terms, i.e. Ω^2 and Ω_{eff}^2 . Right at the bounce, the curvature term reaches its maximum and hence defines a characteristic wavenumber in LQC, namely,

$$k_{\text{LQC}} = \sqrt{\frac{a''}{a}} \Big|_{t=t_B} \approx 3.20, \quad (2.49)$$

where Planck units are used. Comparatively, we find $\Omega^2 \approx 10^{-10}$ and $\Omega_{\text{eff}}^2 = 0.009$ at the bounce. In the second panel, the behavior of the same quantities are compared in the interval $t/t_{\text{Pl}} \in (2 \times 10^4, 4 \times 10^6)$. For $\phi_B/m_{\text{Pl}} = 1.15$, ϕ^2 inflation takes place at $t/t_{\text{Pl}} = 4.64 \times 10^4$. Although near the onset of inflation, the potential term Ω^2 is of similar magnitude with the curvature term, the latter quickly becomes dominant after a few e-folds. In particular, a''/a is about 100 times larger than $\Omega^2/\Omega_{\text{eff}}^2$ at any moment after $t/t_{\text{Pl}} = 1 \times 10^5$. Thus, the comoving Hubble horizon $\lambda_H^2 = 1/s$ is primarily determined by the curvature term during the slow-roll phase. The behavior of $\Omega^2/\Omega_{\text{eff}}^2$ and a''/a in the contracting phase is depicted in the bottom two panels of Fig. 2. In the third panel, the time interval is set to $(-2 \times 10^4, 0)$. Again, near the bounce, the highly oscillating Ω_{eff}^2 is larger than Ω^2 , while both of them are much smaller than the curvature term until $t/t_{\text{Pl}} = -10^4$. The difference between Ω^2 and Ω_{eff}^2 also becomes negligible when $t/t_{\text{Pl}} \leq -10^4$. In the last

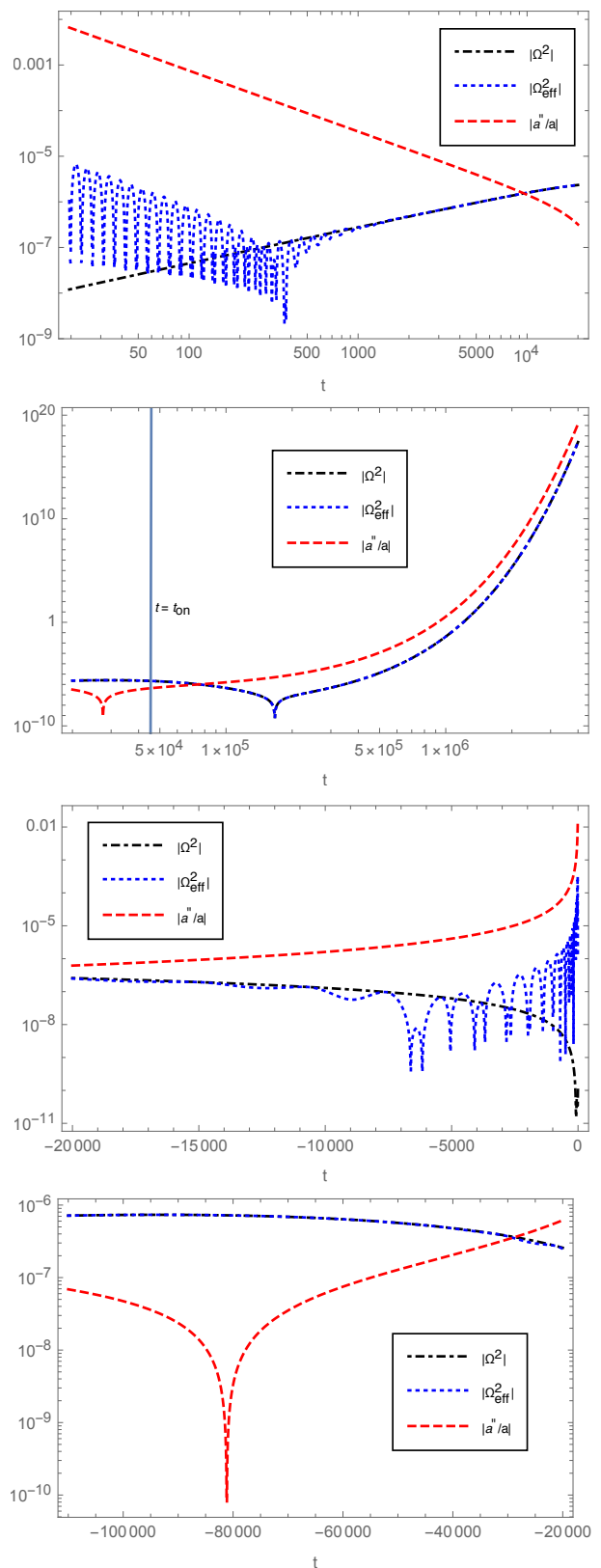


FIG. 2. Setting $\phi_B = 1.15 m_{\text{Pl}}$, we compare the relative magnitude of Ω^2 , Ω_{eff}^2 and a''/a in the whole range $t/t_{\text{Pl}} \in (-1.1 \times 10^5, 4 \times 10^6)$. The top two panels are for the expanding phase, while the bottom two panels are for the contracting phase. In the second panel, the vertical line at $t = t_{\text{on}} = 4.64 \times 10^4$ marks the onset of the inflationary phase. The relative magnitude among Ω^2 , Ω_{eff}^2 and a''/a implies the dominant contribution to the mass squared term in the equation of motion (2.36) and thus plays an important role in comparing different ansatz for Ω^2 .

panel, the time interval is set to $(-1.10 \times 10^5, -2.00 \times 10^4)$. We can see that in this range the potential term and the curvature term are of similar magnitude while the difference between Ω^2 and Ω_{eff}^2 are indistinguishable.

Knowing the details of the potential and curvature terms in both contracting and expanding phases, we can conclude that the main difference between Ω^2 and Ω_{eff}^2 is located near the bounce, specifically, in a region whose boundary is about three e-folds away from the bounce in both expanding and contracting phases. Although right at the bounce, Ω_{eff}^2 is 10^6 times larger than Ω^2 , since the curvature term is overwhelming in this region, the difference between Ω^2 and Ω_{eff}^2 is diluted. Beyond this region, there is no change to the comoving Hubble horizon arising from employing different ansatz of Ω^2 . This indicates that the equation of motion of the perturbations are almost the same for both ansatz except in a small region near the bounce. However, even in this region, the dominant term is the curvature term rather than the potential term. As a result, one might naively expect very tiny changes to the power spectra when switching between two different ansatz. However, to our surprise, the profile of the power spectra still exhibits significant changes in some regimes of the comoving wavenumbers as discussed in the following.

As depicted in Fig. 3, there are three distinctive regimes in the scalar power spectrum as already discussed in LQC [59]:

1. The infrared (IR) regime, which approximately lies in the interval $k/k_* \leq 10^{-4}$. In the figure, the power spectrum in this regime appears to be scale-invariant when $k/k_* \leq 10^{-5}$. However, scale invariance is not an intrinsic property in this regime. It depends on the initial states of the perturbations. As discussed below, when second-order adiabatic states are used as in Fig. 4, the power spectrum keeps decreasing when the wavenumber k decreases. For different Ω^2 , the scalar power spectra exhibit the same order of magnitude which is around 10^{-8} . But, there are indeed some quantitative differences. To be specific, at $k = 5 \times 10^{-6}$, $P_S = 1.69 \times 10^{-8}$ for Ω^2 while $P_S = 1.64 \times 10^{-8}$ for Ω_{eff}^2 . The relative difference in this regime is less than 10% as shown in the second panel of Fig. 3.

2. The intermediate regime, which approximately lies in the interval $10^{-4} \leq k/k_* \leq 1$. This is a regime with characteristic oscillating behavior of the amplified power spectrum. Also in this regime, the most striking difference between Ω^2 and Ω_{eff}^2 can be seen in the figure. In the interval $k/k_* \in (10^{-4}, 10^{-3})$, the relative difference can exceed 100% (the largest value of the relative difference is 200%) due to the spike in the power spectrum resulting from Ω_{eff}^2 .

3. The ultraviolet regime (UV), which starts from $k/k_* \geq 1$. In this regime, the power spectrum becomes scale-invariant and the relative difference between two ansatz become as small as 0.1%. This result is consistent with the former analysis of the comoving Hubble horizon in the slow-roll phase. Before the slow-roll, all the modes

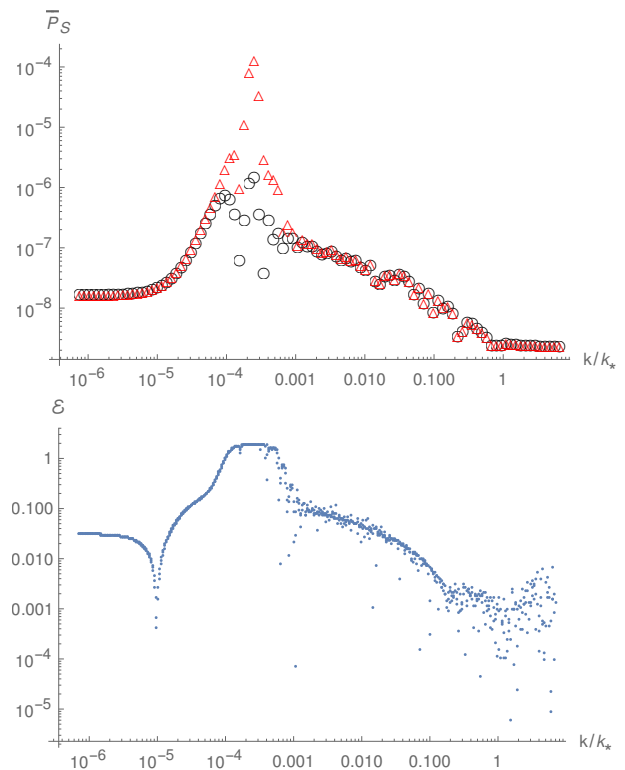


FIG. 3. In LQC, with the initial condition of the background taken to be $\phi_B = 1.15 m_{\text{Pl}}$, the initial states of the perturbations are chosen to be the fourth order adiabatic states which are imposed at $t = -1.1 \times 10^5 t_{\text{Pl}}$. We show the averaged scalar power spectra with respect to small bins of the wavenumber for Ω^2 (black circles) and Ω_{eff}^2 (red triangles), respectively. The wavenumber ranges between $k \in (5 \times 10^{-6}, 50)$ and $k_* = 7.28$ in the figure. In the second panel, the relative difference between two power spectra is defined by $\mathcal{E} = 2|Q_1 - Q_2|/|Q_1 + Q_2|$. Although in the top panel, the black circles are located very close to the the red triangles in the IR regime, their amplitudes are actually not exactly the same. For example, at $k = 5 \times 10^{-6}$, the power spectrum from Ω_{eff}^2 is 1.64×10^{-8} while the power spectrum from Ω^2 is 1.69×10^{-8} . Thus, the relative difference at $k = 5 \times 10^{-6}$ is around 6%.

in this regime are inside the Hubble horizon. They exit the horizon only during the slow-roll. As Ω^2 and Ω_{eff}^2 have the same limit in the slow-roll phase, the power spectra should certainly bear no difference in shape as well as in magnitude.

Other than the initial value $\phi_B = 1.15 t_{\text{Pl}}$ and the 4th-order adiabatic states, we also consider other values of ϕ_B along with other initial states. The main results are summarized in Fig. 4 where Ω^2 is adopted as the effective potential. In the first subfigure of Fig. 4, ϕ_B is still set to $1.15 m_{\text{Pl}}$ at the bounce, while the initial state of the perturbations is changed to the second-order adiabatic state. Its effect on the power spectrum is remarkable in the IR regime. Compared to a scale-invariant IR regime with the 4th-order adiabatic state, the power spectrum

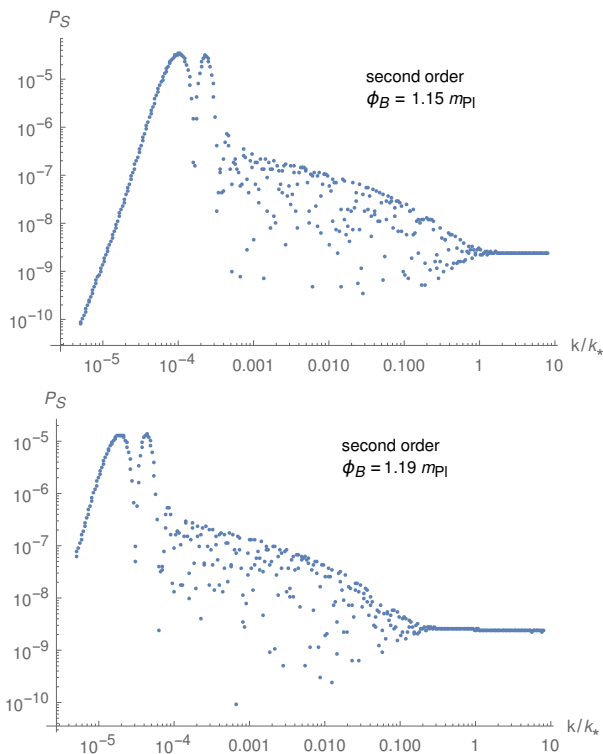


FIG. 4. In this figure, effects of initial conditions of background and the perturbations are examined. In the first subfigure, we only change the initial state of the perturbations to the second-order adiabatic state while keeping $\phi_B = 1.15 m_{\text{Pl}}$. As a consequence, the power spectrum changes its qualitative behavior in the IR regime. In the second panel, we continue with $\phi_B = 1.19 m_{\text{Pl}}$ while keeping the initial state of the perturbations as the second-order adiabatic state. The net effect is to move the observable window to the right as increasing ϕ_B is equivalent to increasing the preinflationary e-folds and thus increasing the value of k_* .

with the second-order adiabatic state is now decreasing when the wavenumber decreases. We thus find that unlike the scale-invariant property of the power spectrum in the UV regime, the property of the power spectrum in the IR regime is sensitive to the property of the initial state. In the second subfigure, we changed the value of ϕ_B to $1.19 m_{\text{Pl}}$. As compared with the first subfigure, the only effect of a different value of ϕ_B is to change the value of k_* and thus move the location of the observable window which is determined by $k/k_* \in (1/8.58, 1000)$ towards the right in the figure. Since the bounce is dominated by the kinetic energy of the inflaton field, such a change of ϕ_B does not produce any significant effect on the scale factor in the bouncing phase. Therefore, the equation of motion of the perturbations are not significantly influenced by the change of ϕ_B . However, as ϕ_B increases, there are now more e-folds from the bounce to the horizon exit of the pivot mode. As a result, k_* is increased and hence the observable window is shifted to the right.

To summarize, in this section, we have compared the power spectrum arising from two different effective potential terms, i.e. Ω^2 and Ω_{eff}^2 . We find the change of the potential can affect the IR and oscillating regimes of the power spectrum even though the magnitude of Ω^2 near the bounce is less than one thousandth of the magnitude of the curvature term a''/a . The influence on the UV regime is quite limited as this part of the power spectrum is mainly determined by the slow-roll phase where Ω^2 and Ω_{eff}^2 become identical to each other. Moreover, the IR behavior of the power spectrum also depends on the initial states of the linear perturbations while the initial conditions of the background would determine the location of the observable window.

III. PRIMORDIAL POWER SPECTRUM IN mLQC-I

In this section, we first give a brief review of the effective dynamics in mLQC-I, focusing on the effective Hamiltonian and the resulting Hamilton's equations. Then we present two different ansatz of $1/\pi_a^2$ when the initial conditions are imposed in the contracting phase. Finally, the scalar power spectra from two ansatz are presented and compared.

A. Review of the effective dynamics in mLQC-I

The mLQC-I model was first proposed as an alternative quantization of the Hamiltonian in LQC and then rediscovered by computing the expectation values of the Hamiltonian constraint in the full loop quantum gravity with complexifier coherent states [45, 46]. This model is characterized by an asymmetric bounce: the contracting branch is an emergent de Sitter phase with an effective Planck-scale cosmological constant and a rescaled Newton's constant. The effective dynamics of this model and modified Friedmann equations were studied in detail in [50], here we present only necessary details. The effective Hamiltonian constraint in this model is explicitly given by

$$\mathcal{H}^1 = \frac{3v}{8\pi G\lambda^2} \left\{ \sin^2(\lambda b) - \frac{(\gamma^2 + 1) \sin^2(2\lambda b)}{4\gamma^2} \right\} + \frac{p_\phi^2}{2v} + vV(\phi) \approx 0, \quad (3.1)$$

from which it is straightforward to derive the Hamilton's equations which are

$$\dot{v} = \frac{3v \sin(2\lambda b)}{2\gamma\lambda} \left\{ (\gamma^2 + 1) \cos(2\lambda b) - \gamma^2 \right\}, \quad (3.2)$$

$$\dot{b} = \frac{3 \sin^2(\lambda b)}{2\gamma\lambda^2} \left\{ \gamma^2 \sin^2(\lambda b) - \cos^2(\lambda b) \right\} - 4\pi G\gamma \left(\frac{p_\phi^2}{2v^2} - V \right). \quad (3.3)$$

While the equations of motion in the matter sector are the same as in LQC given by Eq. (2.31). It can be shown that the bounce takes place at $\dot{H} = 0$ and $\ddot{a} > 0$ when the energy density of the scalar field reaches its maximum value

$$\rho_c^I \equiv \frac{\rho_c}{4(\gamma^2 + 1)}. \quad (3.4)$$

From the Hamilton's equations, the modified Friedmann equation can be derived. It turns out that unlike LQC, the Friedmann equation in the contracting phase is different from the one in the expanding phase, and has higher than quadratic in energy density modifications [50]. More specifically, in the expanding phase,

$$H^2 = \frac{8\pi G\rho}{3} \left(1 - \frac{\rho}{\rho_c^I} \right) \times \left[1 + \frac{\gamma^2 \rho / \rho_c^I}{(\gamma^2 + 1) \left(1 + \sqrt{1 - \rho / \rho_c^I} \right)^2} \right], \quad (3.5)$$

while in the contracting phase,

$$H^2 = \frac{8\pi G\alpha\rho_\Lambda}{3} \left(1 - \frac{\rho}{\rho_c^I} \right) \times \left[1 + \frac{\rho \left(1 - 2\gamma^2 + \sqrt{1 - \rho / \rho_c^I} \right)}{4\gamma^2 \rho_c^I \left(1 + \sqrt{1 - \rho / \rho_c^I} \right)} \right], \quad (3.6)$$

here

$$\alpha \equiv \frac{1 - 5\gamma^2}{\gamma^2 + 1}, \quad \rho_\Lambda \equiv \frac{3}{8\pi G\alpha\lambda^2(1 + \gamma^2)^2}. \quad (3.7)$$

From Eq. (3.6), one can see that $H \rightarrow -\frac{1}{\lambda(1+\gamma^2)} = -0.42$ as long as $\rho \ll \rho_c^I$. Since the energy density drops rather quickly near the bounce, the de Sitter phase becomes a very good approximation just a few Planck seconds before the bounce. From our simulations, we find $H \approx -0.42$ when $t/t_{P1} \leq -2$. Moreover, as compared with LQC, in mLQC-I, the value of $\sin(\lambda b)$ ranges over $[0, \sqrt{1/(\gamma^2 + 1)}]$ with $\sin(\lambda b) = \sqrt{1/(2\gamma^2 + 2)}$ at the bounce. Therefore, $\sin(\lambda b)$ never reaches unity during the entire evolution. In contrast, $b \in (0, \pi/\lambda)$ and $\sin(\lambda b) = 1$ right at the bounce in LQC.

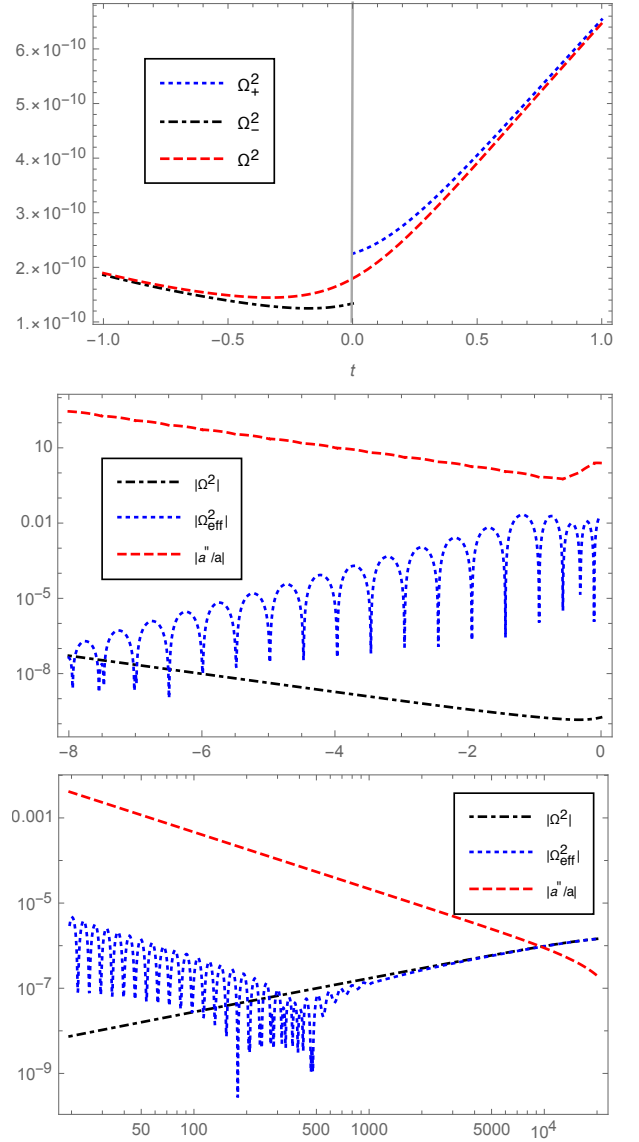


FIG. 5. In the first panel, the potential terms Ω_+^2 , Ω_-^2 are compared with their smooth extension Ω^2 across the bounce in mLQC-I. This smooth extension is achieved by the function $\tilde{\Theta}(b)$ in Eq. (3.11). In the second and third panels, we compare the potential terms Ω^2 and Ω_{eff}^2 with the curvature term a''/a in the whole range where our simulations are carried out. The range of $t \in (2 \times 10^4, 4 \times 10^6)$ is not plotted as these three quantities have the same qualitative behavior as in LQC plotted in Fig. 2.

B. The primordial power spectrum

Similar to LQC, the evolution of the background dynamics is completely fixed by assigning the initial condition of the scalar field at the bounce. In order to compare with LQC and mLQC-II, the value of scalar field at the bounce is set to $\phi_B = 1.27$ and $\dot{\phi}_B > 0$ so that the number of the inflationary e-folds is still 72.8. With this initial condition, the number of the pre-inflationary

e-folds from the bounce to the onset of the inflation is 3.98, which in turn fixes k_* to 5.57. On the other hand, the initial states of the perturbations in mLQC-I are chosen in the contracting branch where the de Sitter phase is a very good approximation. In the de Sitter phase, the equation of motion of the tensor perturbations become

$$\nu'' + \left(k^2 - \frac{2}{\eta^2}\right) \nu = 0, \quad (3.8)$$

where $aH = -1/\eta$ is used. Now in the contracting phase, η must be a positive number as H is negative. Thus, the relation between the conformal time η and the cosmic time t takes the form

$$\eta = \int_{-\infty}^t \frac{dt}{a}. \quad (3.9)$$

Moreover, Eq. (3.8) has the exact solutions which are

$$\nu_k = \alpha_k \frac{e^{-ik\eta}}{\sqrt{2k}} \left(1 - \frac{i}{k\eta}\right) + \beta_k \frac{e^{ik\eta}}{\sqrt{2k}} \left(1 + \frac{i}{k\eta}\right), \quad (3.10)$$

here α_k and β_k are two integration constants. The above solution already indicates that the power spectrum of the super-horizon modes in the slow-roll phase is scale-invariant since $|\nu_k|^2 \propto 1/k^3$ for these modes, while the power spectrum of the comoving curvature perturbations is proportional to $k^3|\nu_k|$. In our simulations, the initial states of the perturbations are chosen as the positive frequency modes with $\alpha_k = 1$ and $\beta_k = 0$.

As the initial conditions of both background and the perturbations are fixed, we now need to figure out the specific ansatz of Ω^2 in Eq. (2.17). The first ansatz comes from the classical background Friedmann constraint, which gives the same Ω_{\pm}^2 by Eq. (2.32) but with background evolution given by effective dynamics of mLQC-I model. As in LQC, Ω_+^2 and Ω_-^2 do not coincide at the bounce which is depicted in the first panel of Fig. 5. Therefore, an extension $\tilde{\Omega}^2$ is required to connect Ω_+^2 with Ω_-^2 smoothly at the bounce. Following our strategy in LQC and using the form of effective Hamiltonian constraint in mLQC-I, we find this extension takes the following form for mLQC-I:

$$\tilde{\Omega}^2 = a^2 \left(V_{,\phi\phi} + 2\tilde{\Theta}(b)fV_{,\phi} + f^2V \right), \quad (3.11)$$

where $\tilde{\Theta}(b) = (1 - 2(\gamma^2 + 1)\sin^2(\lambda b))$ is a monotonous function of b during the evolution of the background. As already discussed in the last subsection, $\sin(\lambda b) \rightarrow \sqrt{1/(1 + \gamma^2)}$ when $t \rightarrow -\infty$ and $\sin(\lambda b) = \sqrt{1/(2 + 2\gamma^2)}$ right at the bounce. Therefore, $\tilde{\Theta}(b)$ monotonously increases from negative unity to zero in the contracting phase. On the other hand, at $t \rightarrow \infty$, $b \rightarrow 0$. This indicates $\tilde{\Theta}(b)$ monotonously increases from zero to positive unity in the expanding phase. As b changes abruptly near the bounce and almost acts like a constant in the other regimes, $\tilde{\Theta}$ behaves like a step function across the bounce as depicted in the first panel of Fig. 5.

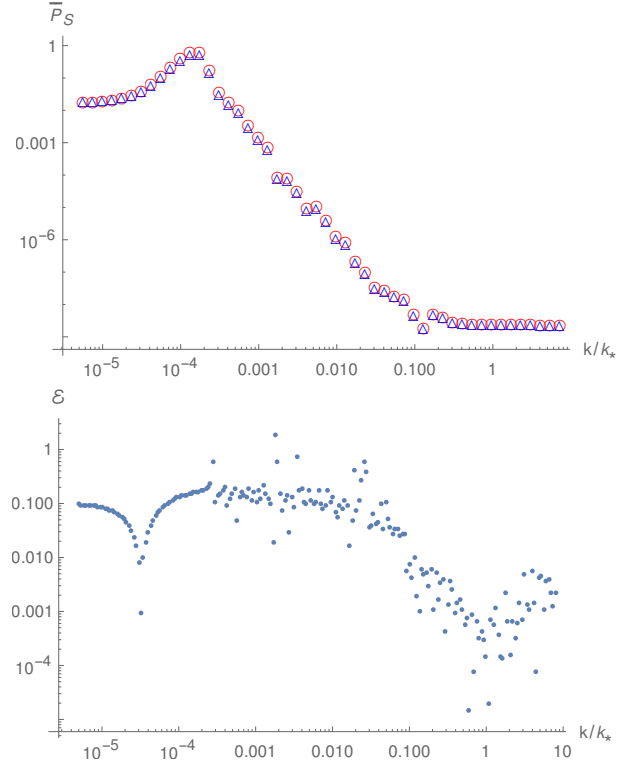


FIG. 6. In mLQC-I, with the value of the scalar field at the bounce set to $1.27 m_{\text{Pl}}$, the initial states of the perturbations are imposed at $t/t_{\text{Pl}} = -2$. The averaged scalar power spectrum is explicitly shown for Ω^2 (blue triangles) and Ω_{eff}^2 (red circles). The relative difference between them is given in the second subfigure. In this figure, $k_* = 5.57$. Two curves in the top panel are actually giving different power spectra in the IR regime. For example, at $k/k_* = 5 \times 10^{-6}$, the power spectrum from Ω_{eff}^2 is 0.017 while the power spectrum from Ω^2 turns out to be 0.019, there is indeed a 10% relative difference.

The second ansatz for Ω^2 comes from the effective Hamiltonian constraint in Eq. (3.1). In mLQC-I, the transition from the classical Hamiltonian constraint to the effective Hamiltonian constraint is achieved by making use of the substitution

$$\frac{1}{\pi_a^2} \rightarrow \frac{64\pi^2 G^2 \lambda^2 \gamma^2}{9a^4 \left[(1 + \gamma^2) \sin^2(2\lambda b) - 4\gamma^2 \sin^2(\lambda b) \right]}. \quad (3.12)$$

The same substitution can now be used in Eq. (2.17), in the same spirit as the procedure in the hybrid approach for LQC [29, 30]. The only subtlety which arises is from the fact that the right hand side of Eq. (3.12) does not equal zero at the bounce. However, with the help of $\tilde{\Theta}(b)$ function introduced in Ω^2 , a proper smooth extension of $1/\pi_a$ across the bounce can be easily found as

$$\frac{1}{\pi_a} \rightarrow -\frac{8\pi G \lambda \gamma \tilde{\Theta}(b)}{3a^2 \sqrt{(1 + \gamma^2) \sin^2(2\lambda b) - 4\gamma^2 \sin^2(\lambda b)}}. \quad (3.13)$$

With the replacements Eqs. (3.12)-(3.13), we obtain the

second ansatz of the potential term, that is, Ω_{eff}^2 . In the last two subfigures of Fig. 5, we compare the relative magnitude of Ω^2 , Ω_{eff}^2 and the curvature term a''/a in the regimes where our simulations of the power spectrum are performed. The middle panel of Fig. 5 tells that in the contracting phase when $t/t_{\text{P1}} \in (-8, 0)$, the curvature term is overwhelming over the potential terms Ω^2 and Ω_{eff}^2 . More specifically, right at the bounce, the curvature term determines a characteristic wavenumber in mLQC-I, which is

$$k_1 = \sqrt{\frac{a''}{a}} \Big|_{t=t_B} \approx 1.60, \quad (3.14)$$

as compared with $\Omega^2 = 1.75 \times 10^{-10}$ and $\Omega_{\text{eff}}^2 = 0.006$ at the bounce. Therefore, the difference between Ω^2 and Ω_{eff}^2 near the bounce are diluted by the background just like in LQC. The last subfigure compares the same three quantities in the interval $t/t_{\text{P1}} \in (0, 2 \times 10^4)$. In the expanding phase, all these quantities behave in a similar way as in Fig. 2. Ω^2 and Ω_{eff}^2 coincide exactly after $t/t_{\text{P1}} = 1000$. While the potential term becomes of similar magnitude with the curvature term near the onset of the inflation, the curvature term quickly exceeds the potential term again during the slow-roll. The behavior of each term in the slow-roll phase is still the same as in the top right panel of Fig. 2, and hence we do not show them explicitly in mLQC-I. From Fig. 5, we can conclude that the difference between Ω^2 and Ω_{eff}^2 lies in the region near the bounce. However, as the curvature term plays a dominant role in this region, one may expect that the impact of the different ansatz of Ω^2 may be undetectable or rather small in the power spectrum. However, in our simulations, we still find around 10% difference in the magnitude of the power spectrum in the IR and oscillating regimes. Now let us proceed with some details of the scalar power spectrum.

The scalar power spectrum in mLQC-I in Fig. 6 for both Ω^2 (blue triangles) and Ω_{eff}^2 (red circles) is in agreement with earlier work [54]. Although the profile of the power spectrum is similar to that in LQC, the magnitude in the IR and oscillating regimes are amplified in great amount as compared with Fig. 3. The magnitude of the power spectrum in the IR regime is actually the result of the de Sitter phase in the contracting phase. In Fig. 7, we plot the comoving Hubble horizon near the bounce which shows that in the de Sitter phase, the horizon is shrinking rapidly backwards in time. As a result, if the initial conditions are imposed in the contracting phase, the IR modes are outside the horizon and their magnitude is frozen. In the de Sitter space, the power spectrum of the superhorizon modes can be simply evaluated by the formula [2]

$$P_S = \frac{1}{4\pi^2} \frac{H^4}{\dot{\phi}^2}, \quad (3.15)$$

which, with $H \approx -0.42$ and $\dot{\phi} \approx 0.03$ (both of them are in the Planck units) in the contracting phase, gives

$P_S \approx 0.88 \approx 1$. Therefore, the large amplitude of the power spectrum in the IR regime in Fig. 6 reflects the existence of a de Sitter phase with a Planck-scale cosmological constant. Whereas, the relatively small magnitude of the power spectrum in the UV regime is actually determined in the slow-roll phase. Using the same expression of P_S in Eq. (3.15) but plugging in the right values of the Hubble rate and $\dot{\phi}$ at the horizon exit in the slow roll, i.e. $H \approx 7.83 \times 10^{-6}$ and $\dot{\phi} \approx 2 \times 10^{-7}$, one immediately obtains $P_S \approx 2.38 \times 10^{-9}$.

Finally we discuss the difference between Ω^2 and Ω_{eff}^2 . The quantitative difference lies near the bounce where the curvature term plays the dominant role. There is still at least a 10% difference in the IR and oscillating regimes of the power spectrum. Near the bounce, the magnitude of Ω_{eff}^2 near the bounce is just one thousandth of that of the curvature term. This difference is actually not as small as expected. In addition to $t/t_{\text{P1}} = -2$, we also impose the initial conditions at different times in the de Sitter phase. The resulting power spectrum is just the same as those in Fig. 6. As discussed above, the IR regime is determined in the contracting phase where its magnitude is frozen outside the horizon and thus insensitive to the time when the initial conditions are chosen.

In summary, in this section, the power spectrum in mLQC-I with the potential terms from the classical and effective constraints was compared with the power spectrum in LQC. The magnitude of the power spectrum in the IR regime is of the order of the Planck scale due to the emergent de Sitter contracting phase. Moreover, different choices of Ω^2 give rise to about 10% relative difference in the IR and oscillating regime which is surprisingly not small, considering the magnitudes of the potential terms Ω^2 , Ω_{eff}^2 are less than one thousandth of the curvature term a''/a near the bounce. Moreover, we also compare the power spectrum from Ω^2 and Ω_+^2/Ω_-^2 in the appendix. Unlike LQC, the discontinuity in Ω_+^2/Ω_-^2 does make a substantial difference even in the UV regime of the power spectrum essentially ruling out mLQC-I unless the discontinuity is cured as discussed previously.

IV. PRIMORDIAL POWER SPECTRUM IN mLQC-II

Similar to mLQC-I, the mLQC-II model was first proposed as an alternative quantization of the Hamiltonian in LQC [45]. Later, the effective dynamics in this model was studied in detail in [48]. It was found that the inflationary phase is still an attractor in the expanding phase when a single scalar field minimally coupled to gravity is introduced. In [4], both numeric and analytic results of the background dynamics were presented in detail. In this section, we first review the effective dynamics in mLQC-II and then present the results of the primordial power spectrum in the dressed metric approach.

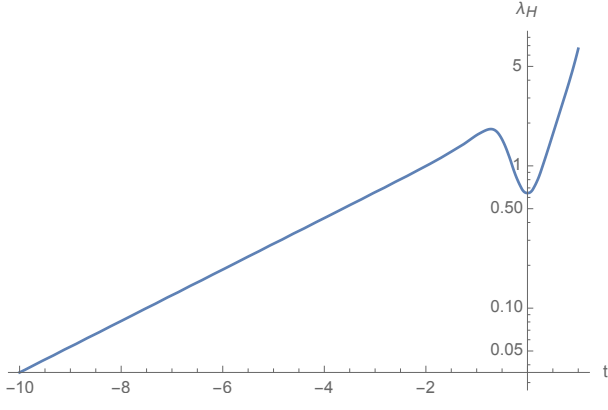


FIG. 7. In mLQC-I, the shape of the comoving Hubble horizon defined by $\lambda_H = \sqrt{a/a''}$ is depicted in the contracting phase and near the bounce in the expanding phase. This figure basically indicates if the initial conditions are set in the contracting phase with Planck scale emergent cosmological constant, the modes with comoving wavelength larger than unity are actually outside the horizon.

A. Review of the effective dynamics in mLQC-II

For the spatially-flat FLRW background, the effective Hamiltonian constraint in mLQC-II is given by [45]

$$\mathcal{H}^{\text{II}} = -\frac{3v}{2\pi G\lambda^2\gamma^2} \sin^2\left(\frac{\lambda b}{2}\right) \left\{ 1 + \gamma^2 \sin^2\left(\frac{\lambda b}{2}\right) \right\} + \frac{p_\phi^2}{2v} + vV(\phi) \approx 0. \quad (4.1)$$

As discussed in Sec. II, the dressed metric approach can be extended to this model in a straightforward way as long as we focus on the background states which are highly peaked on classical trajectories at late times. This is to say, for mLQC-II, the background quantities in Eq. (2.26) are replaced by those from the effective Hamilton's equations given by

$$\dot{v} = \frac{3v \sin(\lambda b)}{\gamma\lambda} \left\{ 1 + \gamma^2 - \gamma^2 \cos(\lambda b) \right\}, \quad (4.2)$$

$$\dot{b} = -\frac{6 \sin^2\left(\frac{\lambda b}{2}\right)}{\gamma\lambda^2} \left\{ 1 + \gamma^2 \sin^2\left(\frac{\lambda b}{2}\right) \right\} - 4\pi G\gamma \left(\frac{p_\phi^2}{2v^2} - V \right). \quad (4.3)$$

The equations of motion of the scalar field and its conjugate momentum are the same as those in LQC given by Eq. (2.31). From the Hamilton's equations, it can be easily shown that the modified Friedmann equation

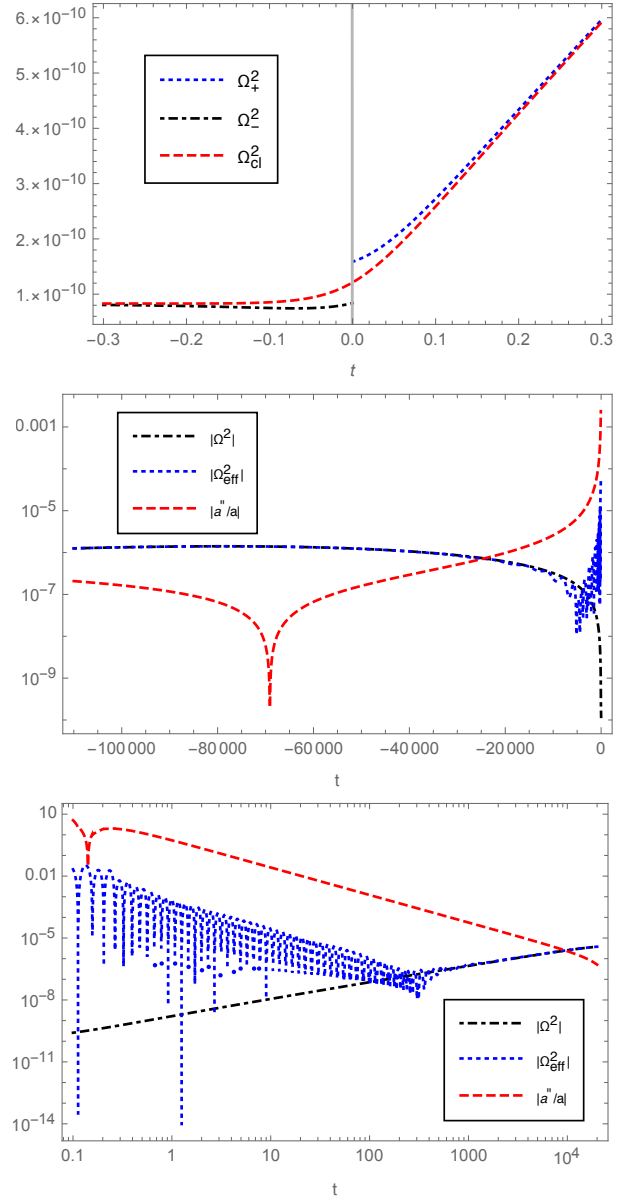


FIG. 8. In mLQC-II, we compare Ω_+^2 , Ω_-^2 and Ω^2 across the bounce in the first figure. Ω^2 smoothly connects Ω_+^2 in the expanding phase with Ω_-^2 in the contracting phase. In the second and the third panels, the difference between Ω^2 and Ω_{eff}^2 is explicitly shown in both contracting and expanding phases. In this figure, $\phi_B = 1.04 m_{\text{Pl}}$ at the bounce.

in mLQC-II takes the form [4]

$$H^2 = \frac{16\pi G\rho}{3} \left(1 - \frac{\rho}{\rho_c^{\text{II}}} \right) \times \left(\frac{1 + 4\gamma^2(\gamma^2 + 1)\rho/\rho_c^{\text{II}}}{1 + 2\gamma^2\rho/\rho_c^{\text{II}} + \sqrt{1 + 4\gamma^2(1 + \gamma^2)\rho/\rho_c^{\text{II}}}} \right). \quad (4.4)$$

In this model, the momentum b monotonously evolves from $2\pi/\lambda$ in the distant past to zero in the future. At the bounce, $b = \pi/\lambda$. Similar to LQC, resulting dynamics

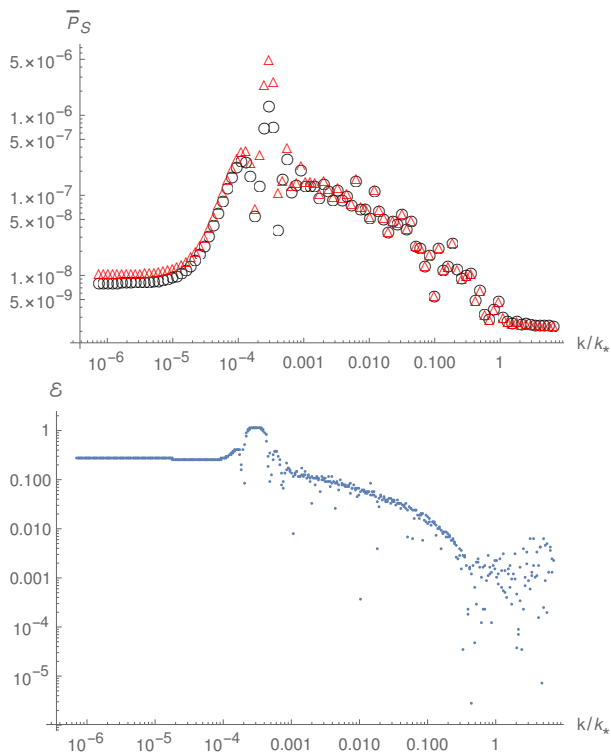


FIG. 9. Setting $\phi_B = 1.04 m_{\text{Pl}}$ at the bounce in mLQC-II. The initial states of the perturbations are chosen to be the 4th order adiabatic states given in Eq. (2.45). The power spectra from Ω^2 (black circles) and Ω_{eff}^2 (red triangles) are compared in the first panel. In the second panel, the relative difference between two power spectra is given. Although two curves in the top panel are located very close to each other, the relative difference in the IR regime turns out to be larger than that in LQC. To be more specific, we find that at $k = 5 \times 10^{-6}$, the power spectrum from Ω_{eff}^2 is 1.07×10^{-8} while the power spectrum from Ω^2 is 8.10×10^{-9} , so the relative difference is up to 28%.

also describes a bouncing universe in which the bounce takes place when the energy density of the scalar field reaches its maximum value at

$$\rho_c^{\text{II}} \equiv 4(\gamma^2 + 1)\rho_c. \quad (4.5)$$

The evolution of the universe is symmetric about the bounce point as in LQC.

B. The primordial power spectrum

As the qualitative behavior of the background dynamics in mLQC-II is quite similar to that in LQC, we follow the same procedure to analyze the power spectrum in mLQC-II. First, the initial conditions of the background in mLQC-II are chosen to be $\phi_B = 1.04 m_{\text{Pl}}$ and $\dot{\phi}_B > 0$ at the bounce. As a result, the number of e-folds from the bounce to the onset of inflation is 4.46 and the number of inflationary e-folds is 72.8 which is the same as

in LQC when $\phi_B^{\text{LQC}} = 1.15 m_{\text{Pl}}$. The pivot mode computed from $k_* = a_* H_*$ at the horizon exit turns out to be $k_* = 9.54$. Meanwhile, the initial states of the perturbations are chosen to be the 4th order adiabatic states in Eq. (2.40) at the moment $t/t_{\text{Pl}} = -1.1 \times 10^5$. The only complications come from the Ω^2 term in the mass squared term s in Eq. (2.44). Two different candidates are studied in the following: Ω^2 coming from the classical background Hamiltonian constraint and Ω_{eff}^2 from the effective Hamiltonian constraint. Ω^2 is given by

$$\Omega^2 = a^2 (V_{,\phi\phi} + 2\Theta(b)fV_{,\phi} + f^2V), \quad (4.6)$$

here $\Theta(b) = \cos(\lambda b/2)$ behaves like a step function across the bounce and picks up the right sign in both contracting and expanding phases. Eq. (4.6) is thus a smooth extension of Eq. (2.32) into the contracting phase in mLQC-II. On the other hand, Ω_{eff}^2 is given by comparing the classical background Hamiltonian constraint in Eq. (2.7) with the effective Hamiltonian constraint Eq. (4.1), which leads to the following replacements of $1/\pi_a^2$ and $1/\pi_a$:

$$\frac{1}{\pi_a^2} \rightarrow \frac{4\pi^2\gamma^2\lambda^2}{9a^4 \sin^2(\lambda b/2) (1 + \gamma^2 \sin^2(\lambda b/2))}, \quad (4.7)$$

$$\frac{1}{\pi_a} \rightarrow \frac{-2\pi\gamma\lambda \cos(\lambda b/2)}{3a^2 \sin(\lambda b/2) \sqrt{(1 + \gamma^2 \sin^2(\lambda b/2))}}. \quad (4.8)$$

In Fig. 8, we first compare Ω_+^2, Ω_-^2 with their smooth extension Ω^2 near the bounce. As can be seen from this figure, Ω^2 quickly tends to Ω_+^2/Ω_-^2 in the expanding/contracting phase within 0.5 Planck second. This is because the momentum b changes dramatically from its maximum to the minimum near the bounce due to which $\Theta(b) = \cos(\lambda b/2)$ acts like a step function across the bounce. In the second and third panels of Fig. 8, we compare $\Omega^2, \Omega_{\text{eff}}^2$ with the curvature term in the region where our simulations are performed. The curvature term keeps its dominant role near the bounce. To be more specific, right at the bounce, $\Omega^2 = 1.59 \times 10^{-10}$, $\Omega_{\text{eff}}^2 = 0.265$, which are in contrast with the curvature term $a''/a = 46.8$. In mLQC-II, the characteristic wavenumber at the bounce is

$$k_{\text{II}} = \sqrt{\frac{a''}{a}} \Big|_{t=t_B} \approx 6.84. \quad (4.9)$$

In the contracting(expanding) phase, Ω^2 and Ω_{eff}^2 tend to the same limit before $t/t_{\text{Pl}} = -10^4$ (after $t/t_{\text{Pl}} = 1000$) which is again about 3 e-foldings away from the bounce. At $t/t_{\text{Pl}} \approx -10^5$ and the onset of inflation, the potential terms become comparable to the curvature term. All these properties are quite similar to those of LQC discussed in Sec. II. In Fig. 9, we compare the power spectrum from Ω^2 and Ω_{eff}^2 in the region $k \in (5 \times 10^{-6}, 50)$. We find that the relative difference in the magnitude of the power spectrum is around 30% in the IR regime and less than 10% in the

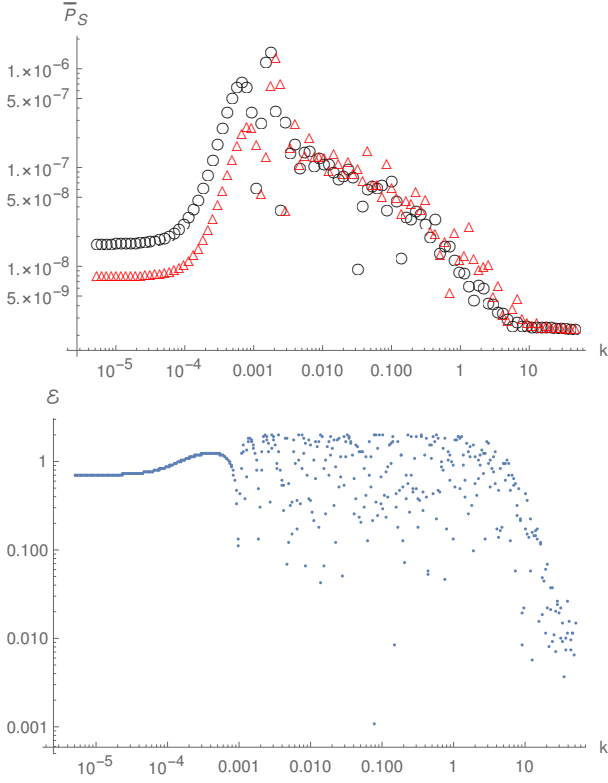


FIG. 10. The scalar power spectra from the classical background Hamiltonian constraint in LQC (black circles) and mLQC-II (red triangles) are compared, the relative difference in the second panel shows the difference of the power spectrum in these two models mainly lies in the IR and oscillating regimes.

intermediate regime except around the spike at the end of the IR regime. Note that Ω_{eff}^2 is able to result in a higher spike than Ω^2 in the power spectrum. Near the spike, the relative difference can exceed even 100%. As the wavenumber becomes closer to k_* , the relative difference decreases. In the UV regime, the relative difference can be as small as 0.1% and even less. In Figs. 10-11, we compare the power spectrum with the same Ω^2 in LQC and mQLC-II. In these figures, the relative difference between LQC and mQLC-II with the same regularization of π_a can be as large as 100% throughout the IR and oscillating regimes. Note the horizontal axis in these plots is the wavenumber not the ratio k/k_* , because k_* is different in two different models, if we keep the same e-foldings of the inflationary phase. Basically, from the analysis in LQC, the change of ϕ_B would only affect the location of the observable window in the power spectrum. Therefore, for other ϕ_B , one would get the same results as plotted in Figs. 10-11. From these figures, we learn that different quantizations of the Lorentzian term in the effective Hamiltonian cause in general more pronounced effects than the different regularizations of π_a in the dressed metric approach, except the regime of spike in power spectrum between IR

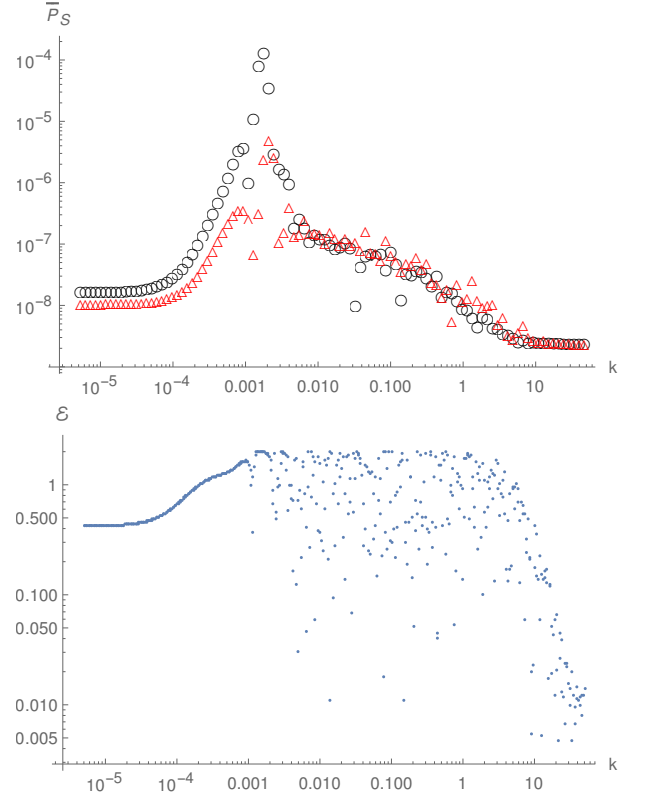


FIG. 11. The scalar power spectra from the effective constraint Ω_{eff}^2 in LQC (black circles) and mLQC-II (red triangles) are compared.

and oscillatory regimes discussed above. In particular, the former can cause a relative difference exceeding 100% even in the intermediate regime while the relative difference caused by different Ω^2 is generally less than 30% in the same regime.

So far we have discussed the scalar power spectrum in different models. Finally, in Fig. 12, we compare the tensor power spectra from three models when the initial conditions of the background are set so that the e-foldings of the inflationary phase is 72.8 in all three models. As can be seen from the figure, the power spectrum in mLQC-I again bears traits of the de Sitter phase in the contracting branch with a large cosmological constant as the magnitude of the power spectrum in the IR regime is still of the Planck scale. This is due to the Planck scale valued Hubble rate in the contracting phase and also the fact that the IR regime is frozen during the bouncing and the expanding phases. On the other hand, the tensor power spectrum in LQC and mLQC-II is qualitatively similar, which is featured by a larger magnitude in the IR regime as compared with the scalar power spectrum. The difference between LQC and mLQC-II in the oscillating regime is also striking as the relative difference is more than 50%. All these differences are essentially caused by different background evolutions in these two models, which

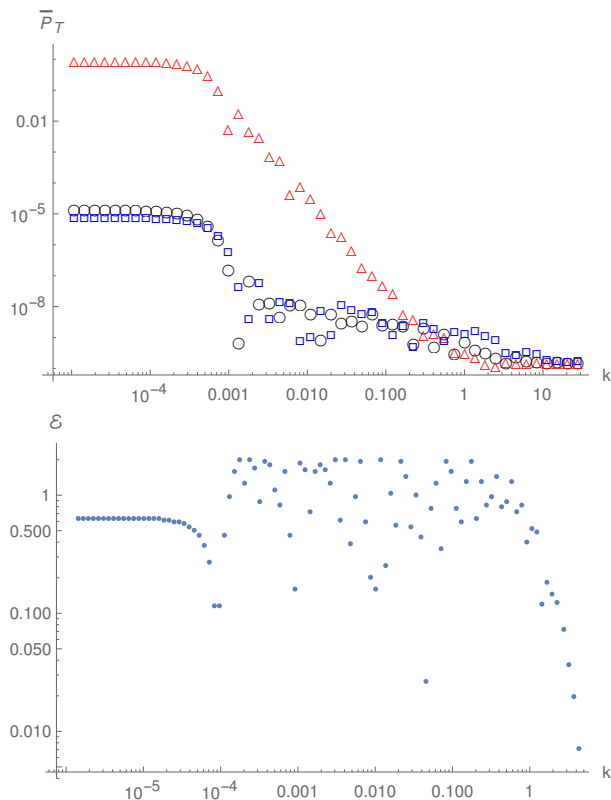


FIG. 12. Tensor power spectra from three models: LQC (black circles), mLQC-I (red triangles), mLQC-II (blue squares). The bottom panel shows the relative difference between LQC and mLQC-II.

again implies quantization ambiguity in the Hamiltonian constraint is able to cause distinguishable effects in both scalar and tensor power spectrum.

V. SUMMARY

In this paper, we have applied the dressed metric approach to cosmological perturbations to compare power spectrum in three loop cosmological models, LQC, mLQC-I and mLQC-II. They result from different regularizations of the Lorentzian term in the classical Hamiltonian constraint [45]. Our first goal was to understand the way different regularizations of the Hamiltonian constraint affect primordial scalar and tensor power spectrum for the chaotic inflationary scenario in a spatially-flat universe. Our second goal was to understand effects of an ambiguity in the dressed metric approach related to the way π_a is treated in the effective potential given in Eq (2.17). We used two different ways to regularize this term: the first ansatz is the conventional treatment used in dressed metric approach [28] which involves solving in part the classical background Hamiltonian constraint for π_a . The second ansatz inspired by the hybrid approach to cosmological perturbations in LQC [29, 30] is obtained

using the effective Hamiltonian constraint in each model. While effects on primordial power spectrum for LQC as well as mLQC-I were studied earlier, a detailed comparison of different regularizations, and effects of above ambiguities have been explored for the first time. Further, unlike majority of works so far in the dressed metric approach, we consider initial conditions in the contracting branch which requires addressing certain subtleties in a discontinuity in the perturbation equations for the dressed metric approach.

From the simulations of the power spectrum, we find that in the UV regime, all three models as well as two different ansatz of π_a give essentially the same scale-invariant power spectrum consistent with the CMB observations [58]. However, there can be significant differences in the IR and intermediate regimes. The magnitude of the power spectrum in the IR regime is slightly higher in LQC when compared to mLQC-II. But, the relative difference between the amplitude of oscillations in these two models can be as large as 50% throughout the IR and intermediate regimes. In mLQC-I, we generalize the results of [54] to understand the effect of ambiguities in considering different π_a in various regimes. The magnitude of the power spectrum is of the order of Planck scale in the IR regime and also in part of the oscillating regime. This feature in mLQC-I is essentially a result of the Planck scale cosmological constant in the pre-bounce regime. We find that different ansatz of π_a in each model result in relative difference of amplitude of at least 10% in the IR regime. And, this difference can be very large, reaching even 100%, for a short range near the interface of IR and oscillatory regime. Except in this short regime, the relative difference between different models with the same ansatz of π_a is always larger than the relative difference between different ansatz of π_a in the same model. This is expected because the effective potential term is at least three orders of magnitude smaller than the curvature term near the bounce. Meanwhile, two ansatz of π_a tend to the same classical limits when they are still much smaller as compared with the curvature term. As a result, the effects of different ansatz of π_a are relatively suppressed in the power spectrum as compared with the choice of different regularization leading to differences in background dynamics except near the border of IR and oscillatory regime. For the sub-horizon modes, differences between choices of π_a turn out to be less than 1%.

In addition, the effects of the initial conditions on the power spectrum in all three models are similar and can be summarized as follows. For the kinetic dominated bounce, the background dynamics in the bouncing phase is not sensitive to ϕ_B at the bounce, and as a result, a change of ϕ_B only affects the pre-inflationary e-folds from the bounce to the horizon exit. This results in moving the observable window to the left (decreasing ϕ_B) or the right (increasing ϕ_B) in the profile of the power spectrum. The effects of the choice of initial states of the perturbations can be seen in the IR regime of the power spectrum for LQC and mLQC-II. Generally, for the zeroth and

second order adiabatic states, the power spectrum keeps decreasing as the comoving wavenumber decreases, while for the 4th-order adiabatic states, the power spectrum is again scale-invariant in the IR regime when $k/k_* \leq 10^{-5}$. For mLQC-I, the power spectrum is scale-invariant in the latter regime because of the de Sitter phase.

We investigated effects of a small discontinuity at the bounce in the equations of motion captured by potentials Ω_{+}^2 and Ω_{-}^2 in the expanding and contracting branches respectively. Motivated by the procedure in the hybrid approach, we performed a smooth interpolation to obtain a potential Ω^2 . Effects of above discontinuity and robustness of our approximation were investigated by comparing the power spectrum resulting from Ω_{\pm}^2 and Ω^2 (see Appendix). The relative difference in the power spectrum produced by these two effective potentials, Ω_{\pm}^2 and Ω^2 , are small in both LQC and mLQC-II. The relative error is around 0.1% in the UV regime and almost negligible in the IR and the oscillatory regimes. However, in mLQC-I, the discontinuity in the equation of motion of the perturbations at the bounce results in a discontinuity in the power spectrum just before the mode $k = k_*$. This discontinuity causes the power spectrum in the UV regime to become extremely large which is excluded by the CMB observations. This result shows that even a seemingly small discontinuity resulting from mismatch between Ω_{+}^2 and Ω_{-}^2 essentially rules out the model unless one uses the smooth potential Ω^2 . For the latter choice, one obtains a scale-invariant spectrum with correct amplitude in the UV regime.

In summary, our analysis shows that although LQC, mLQC-I and mLQC-II give the same power spectrum in the UV regime, the relative differences in the IR and intermediate regimes are far from negligible. To be more specific, the relative differences in the magnitude of the power spectra in LQC and mLQC-II can be larger than 50% throughout the IR and intermediate regimes, while the magnitude of the power spectrum in mLQC-I is of the Planck scale. Furthermore, two regularizations of π_a can also cause at least 10% relative difference in magnitude, in particular, the relative difference in mLQC-II can exceed 20% in the IR regime. We expect that these results are robust to changes in inflationary potential. In future, it will be interesting to address how to differentiate these models, as well as the choices of π_a , from observational perspective. Since all these differences are related with the modes that are outside the current Hubble horizon, effects of the amplified power spectrum in the IR and oscillating regimes may only be indirectly observed by studying the non-Gaussianity in these models. Thus, CMB can serve as an important tool to distinguish effects due to regularizations and quantization ambiguities. The way these effects translate to phenomenological differences for the modes in our observable universe, will be explored in a future work.

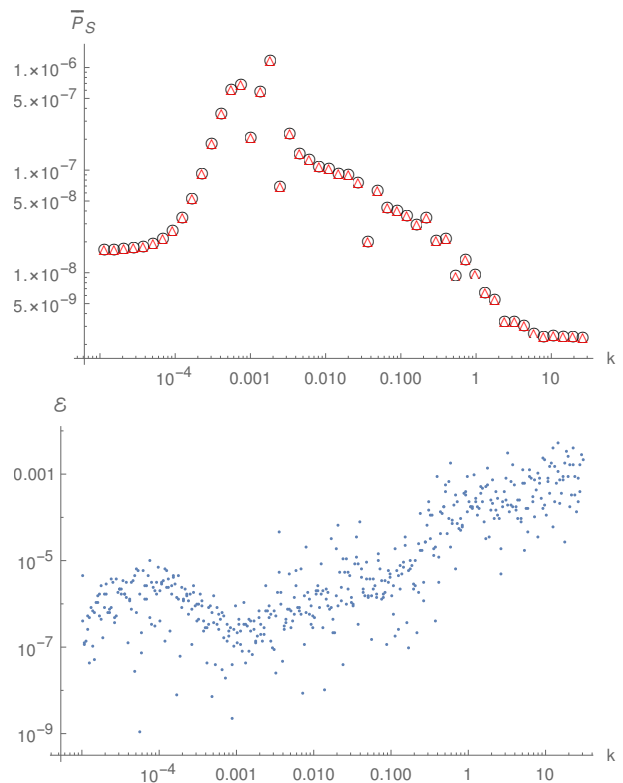


FIG. 13. In LQC, using the 4th-order adiabatic states and setting $\phi = 1.15 m_{Pl}$, the power spectra with smoothly extended Ω^2 (black circles) and discontinuous one Ω_{\pm}^2 (red triangles) introduced in Eq. (A.3) are compared. The relative difference of the resulting power spectrum is almost negligible in the IR and oscillating regimes while in the UV regime, there is around 0.1% difference with these two ansatz.

ACKNOWLEDGEMENTS

We are grateful to Javier Olmedo for extensive discussions and helpful comments. We also thank Sahil Saini and Tao Zhu for discussions. A.W. and B.F.L. are supported in part by the National Natural Science Foundation of China (NNSFC) with the Grants Nos. 11847216, 11375153 and 11675145. P.S. is supported by NSF grant PHY-1454832.

Appendix A: The power spectrum from the discontinuous effective potential

This appendix deals with investigating effects of using a discontinuous effective potential constructed from Ω_{+}^2 and Ω_{-}^2 in the equations for perturbations for LQC, mLQC-I and mLQC-II. Comparison is then made with potential obtained by a smooth interpolation Ω^2 introduced earlier in different models.

As discussed in LQC, in the expanding phase, the effective potential term takes the form

$$\Omega_{+}^2 = a^2 (V_{,\phi\phi} + 2fV_{,\phi} + f^2V), \quad (\text{A.1})$$

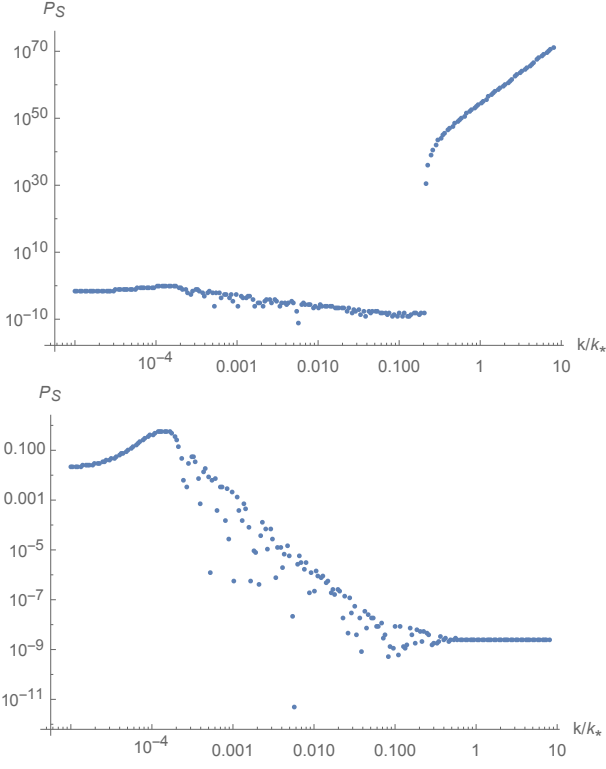


FIG. 14. In mLQC-I, the power spectra with discontinuous Ω_{\pm}^2 (top panel) and smoothly extended Ω^2 (bottom panel) are presented. It is remarkable that the tiny discontinuity at the bounce in Ω_{\pm}^2 gives rise to a huge discontinuity of the power spectrum at around $k = k_*$ and also makes the power spectrum divergent in the UV regime.

while in the contracting phase, as the momentum π_a changes its sign, the effective potential becomes

$$\Omega_-^2 = a^2 (V_{,\phi\phi} - 2fV_{,\phi} + f^2V). \quad (\text{A.2})$$

The difference between Ω_+^2 and Ω_-^2 at the bounce is just around 10^{-10} in LQC and also in mLQC-I/II. Considering that the magnitude of the curvature term at the bounce is always of the order of the Planck scale, one may naively conclude that this small gap of 10^{-10} is almost negligible in all three models, and thus instead of the smooth extension Ω^2 , the ansatz

$$\Omega_{\pm}^2 = a^2 (V_{,\phi\phi} + 2 \text{sgn}(t)fV_{,\phi} + f^2V), \quad (\text{A.3})$$

can also be employed in the simulations of the power spectrum. Here $\text{sgn}(t)$ is a sign factor which takes unity in the expanding phase, and equals negative one in the contracting phase. The results with Ω_{\pm}^2 are compared in Figs. 13-15 with the power spectrum obtained using Ω^2 introduced earlier for each model. As can be seen in Fig. 13, in LQC, Ω_{\pm}^2 and Ω^2 generate almost the same power spectrum in the IR, oscillating and UV regimes.

The relative difference between these two ansatz is almost negligible in the IR regime, the largest error takes

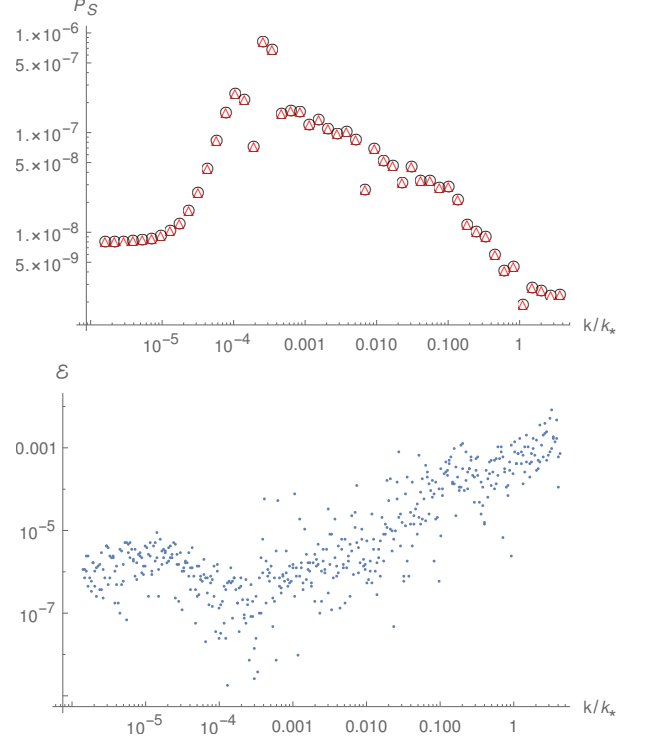


FIG. 15. In mLQC-II, using the 4th-order adiabatic state and setting $\phi = 1.04 m_{\text{Pl}}$, the power spectra with smoothly extended Ω^2 (black circles) and discontinuous one Ω_{\pm}^2 (red triangles) are compared. Similar to LQC, two ansatz of Ω_{\pm}^2 and Ω_{eff}^2 do not make an essential difference in all three regimes of the power spectrum.

place in the UV regime which is around 0.1%. This indicates the discontinuity of the effective potential in LQC at the bounce would not make a substantial difference in the prediction of the power spectrum. One can use either Ω_{\pm}^2 or Ω^2 for the purpose of calculating the power spectrum. However, this is not the case for mLQC-I. The plots in Fig. 14 are the power spectrum in mLQC-I. In the first subfigure, the power spectrum has a discontinuity at around $k = k_*$ and then blows up in the UV regime when the discontinuous potential Ω_{\pm}^2 is employed in the simulations, while the second figure is for the power spectrum with the continuous extension Ω^2 . So it is striking to see that a tiny discontinuity in the background can cause such a huge difference in the UV regime of the power spectrum. If one does not use a continuous potential term in this case, the model would be ruled out due to a tiny discontinuity. This discontinuity and resulting effects in the power spectrum motivates one to consider smoothly interpolated potential such as Ω^2 for all the models. The situation in mLQC-II is very similar to LQC as can be seen from Fig. 15. As in LQC, in this model the discontinuity in Ω_{\pm}^2 does not cause any significant effect in the primordial power spectrum.

- [1] A. H. Guth, *Inflationary universe: A possible solution to the horizon and flatness problems*, Phys. Rev. D **23** 347 (1981).
- [2] D. Baumann, *TASI Lectures on Inflation*, arXiv:0907.5424.
- [3] Z.-K. Guo, D. J. Schwarz, and Y.-Z. Zhang, *Observational constraints on the energy scale of inflation*, Phys. Rev. D **83** 083522 (2011).
- [4] B.F. Li, P. Singh, A. Wang, *Genericness of pre-inflationary dynamics and probability of the desired slow-roll inflation in modified loop quantum cosmologies*, Phys. Rev. D **100**, 063513 (2019).
- [5] C. Rovelli, *Quantum gravity* (Cambridge University Press, London, 2004); A. Ashtekar and J. Lewandowski, *Background independent quantum gravity: a status report*, Class. Quant. Grav. **21**, R53 (2004); T. Thiemann, *Canonical quantum general relativity* (Cambridge University Press, London, 2007); R. Gambini and J. Pullin, *A first course in loop quantum gravity* (Oxford University Press, New York, 2011).
- [6] M. Bojowald, *Loop quantum cosmology*, Living Rev. Relativity **11**, 4 (2008); A. Ashtekar and P. Singh, *Loop Quantum Cosmology: A Status Report*, Class. Quant. Grav. **28**, 213001 (2011).
- [7] A. Ashtekar, T. Pawłowski. and P. Singh, *Quantum nature of the big bang*, Phys. Rev. Lett **96**, 141301 (2006).
- [8] A. Ashtekar, T. Pawłowski and P. Singh, *Quantum Nature of the Big Bang: An Analytical and Numerical Investigation. I.*, Phys. Rev. D **73**, 124038 (2006).
- [9] A. Ashtekar, T. Pawłowski. and P. Singh, *Quantum nature of the big bang: Improved dynamics*, Phys. Rev. D **74**, 084003 (2006).
- [10] A. Ashtekar, A. Corichi. and P. Singh, *Robustness of key features of loop quantum cosmology*, Phys. Rev. D **77**, 024046 (2010).
- [11] P. Diener, B. Gupt and P. Singh, *Numerical simulations of a loop quantum cosmos: robustness of the quantum bounce and the validity of effective dynamics*, Class. Quant. Grav. **31**, 105015 (2014).
- [12] P. Diener, B. Gupt, M. Megevand and P. Singh, *Numerical evolution of squeezed and non-Gaussian states in loop quantum cosmology*, Class. Quant. Grav. **31**, 165006 (2014).
- [13] P. Diener, A. Joe, M. Megevand and P. Singh, *Numerical simulations of loop quantum Bianchi-I spacetimes*, Class. Quant. Grav. **34**, 094004 (2017).
- [14] P. Singh, *Are loop quantum cosmos never singular?*, Class. Quant. Grav. **26**, 125005 (2009); P. Singh, *Loop quantum cosmology and the fate of cosmological singularities*, Bull. Astron. Soc. India **42**, 121 (2014).
- [15] I. Agullo and P. Singh, *Loop Quantum Cosmology*, in *Loop Quantum Gravity: The First 30 Years*, Eds: A. Ashtekar, J. Pullin, World Scientific (2017) arXiv:1612.01236.
- [16] P. Singh, K. Vandersloot, and G. V. Vereshchagin, *Non-singular bouncing universes in loop quantum cosmology*, Phys. Rev. D **74**, 043510 (2006).
- [17] A. Ashtekar and D. Sloan, *Probability of Inflation in Loop Quantum Cosmology*, Gen. Relativ. Gravit. **43**, 3619 (2011).
- [18] A. Corichi, A. Karami, *On the measure problem in slow roll inflation and loop quantum cosmology*, Phys. Rev. D **83**, 104006 (2011).
- [19] E. Ranken and P. Singh, *Non-singular Power-law and Assisted inflation in Loop Quantum Cosmology*, Phys. Rev. D **85**, 104002 (2012) doi:10.1103/PhysRevD.85.104002.
- [20] B. Bonga and B. Gupt, *Inflation with the Starobinsky potential in Loop Quantum Cosmology*, Gen. Rel. Grav. **48**, 71 (2016)
- [21] B. Gupt and P. Singh, *A quantum gravitational inflationary scenario in Bianchi-I spacetime*, Class. Quant. Grav. **30**, 145013 (2013).
- [22] S. Tsujikawa, P. Singh, R. Maartens, *Loop quantum gravity effects on inflation and the CMB*, Class. Quant. Grav. **21**, 5767 (2004); G. M. Hossain, *Primordial density perturbation in effective loop quantum cosmology*, Class. Quant. Grav. **22**, 2511 (2005); D. J. Mulryne and N. J. Nunes, *Constraints on a scale invariant power spectrum from superinflation in LQC*, Phys. Rev. D **74**, 083507 (2006); M. Bojowald et al., *Formation and Evolution of Structure in Loop Cosmology*, Phys. Rev. Lett **98**, 031301 (2007); J. Magueijo and P. Singh, *Thermal fluctuations in loop cosmology*, Phys. Rev. D **76**, 023510 (2007); G. Calcagni and M. Cortes, *Inflationary scalar spectrum in loop quantum cosmology*, Class. Quant. Grav. **24**, 829 (2007).
- [23] M. Bojowald, G. M. Hossain, M. Kagan, S. Shankaranarayanan, *Anomaly freedom in perturbative loop quantum gravity*, Phys. Rev. D **78**, 063547 (2008).
- [24] T. Cailleteau, A. Barrau, J. Grain, F. Vidotto, *Consistency of holonomy-corrected scalar, vector and tensor perturbations in Loop Quantum Cosmology*, Phys. Rev. D **86**, 087301 (2012).
- [25] T. Cailleteau, J. Mielczarek, A. Barrau, J. Grain, *Anomaly-free scalar perturbations with holonomy corrections in loop quantum cosmology*, Class. Quant. Grav. **29**, 095010 (2012).
- [26] I. Agullo, A. Ashtekar and W. Nelson, *Quantum gravity extension of the inflationary scenario*, Phys. Rev. Lett. **109**, 251301 (2012).
- [27] I. Agullo, A. Ashtekar and W. Nelson, *Extension of the quantum theory of cosmological perturbations to the Planck era*, Phys. Rev. D **87**, 043507 (2013).
- [28] I. Agullo, A. Ashtekar and W. Nelson, *The pre-inflationary dynamics of loop quantum cosmology: confronting quantum gravity with observations*, Class. Quant. Grav. **30**, 085014 (2013).
- [29] M. F.-Mendez and G. A. M. Marugan, *Hybrid quantization of an inflationary model: The flat case*, Phys. Rev. D **88**, 044013 (2013).
- [30] L.C. Gomar, M. F.-Mendez, G. A. M. Marugan and J. Olmedo, *Cosmological perturbations in hybrid loop quantum cosmology: Mukhanov-Sasaki variables*, Phys. Rev. D **90**, 064015 (2014).
- [31] L.C. Gomar, M. M.-Benito, G. A. M. Marugan, *Gauge-invariant perturbations in hybrid quantum cosmology*, JCAP **1506** (2015) 06, 045.
- [32] E. Wilson-Ewing, *Testing loop quantum cosmology*, Comptes Rendus Physique **18**, 207 (2017).
- [33] A. Ashtekar and B. Gupt, *Quantum Gravity in the Sky: Interplay between fundamental theory and observations*, Class. Quant. Grav. **34**, no. 1, 014002 (2017).

- [34] A. Ashtekar and B. Gupt, *Initial conditions for cosmological perturbations*, *Class. Quant. Grav.* **34**, 035004 (2017)
- [35] I. Agullo, A. Ashtekar and B. Gupt, *Phenomenology with fluctuating quantum geometries in loop quantum cosmology*, *Class. Quant. Grav.* **34**, 074003 (2017).
- [36] D. M. de Blas and J. Olmedo, *Primordial power spectra for scalar perturbations in loop quantum cosmology*, *JCAP* **1606**, 029 (2016).
- [37] B. Bonga and B. Gupt, *Phenomenological investigation of a quantum gravity extension of inflation with the Starobinsky potential*, *Phys. Rev. D* **93**, 063513 (2016)
- [38] L. Castell Gomar et al., *Hybrid loop quantum cosmology and predictions for the cosmic microwave background*, *Phys. Rev. D* **96**, 103528 (2017).
- [39] T. Zhu, A. Wang, G. Cleaver, K. Kirsten, and Q. Sheng, *Pre-inflationary universe in loop quantum cosmology*, *Phys. Rev. D* **96**, 083520 (2017); T. Zhu, A. Wang, K. Kirsten, G. Cleaver, and Q. Sheng, *Universal features of quantum bounce in loop quantum cosmology*, *Phys. Lett. B* **773** (2017) 196.
- [40] T. Zhu, A. Wang, K. Kirsten, G. Cleaver, and Q. Sheng, *Primordial non-Gaussianity and power asymmetry with quantum gravitational effects in loop quantum cosmology*, *Phys. Rev. D* **97**, 043501 (2018); Q. Wu, T. Zhu, and A. Wang, *Nonadiabatic evolution of primordial perturbations and non-Gaussianity in hybrid approach of loop quantum cosmology* *Phys. Rev. D* **98**, 103528 (2018).
- [41] I. Agullo, B. Bolliet and V. Sreenath, *Non-Gaussianity in loop quantum cosmology*, *Phys. Rev. D* **97**, 066021 (2018).
- [42] B. E. Navascues, D. M. de Blas and G. A. M. Marugan, *Time-dependent mass of cosmological perturbations in the hybrid and dressed metric approaches to loop quantum cosmology*, *Phys. Rev. D* **97**, 043523 (2018).
- [43] A. Ashtekar, B. Gupt, D. Jeong and V. Sreenath, *Alleviating the tension in CMB using Planck-scale Physics*, arXiv:2001.11689 [astro-ph.CO].
- [44] A. Ashtekar, W. Kaminski and J. Lewandowski, *Quantum field theory on a cosmological, quantum space-time*, *Phys. Rev. D* **79**, 064030 (2009).
- [45] J. Yang, Y. Ding and Y. Ma, *Alternative quantization of the Hamiltonian in loop quantum cosmology II: Including the Lorentz term*, *Phys. Lett. B* **682** (2009) 1.
- [46] A. Dapor and K. Liegener, *Cosmological Effective Hamiltonian from full Loop Quantum Gravity Dynamics*, *Phys. Lett. B* **785** (2018) 506.
- [47] S. Saini, P. Singh, *Generic absence of strong singularities and geodesic completeness in modified loop quantum cosmologies*, arXiv:1812.08937.
- [48] B.F. Li, P. Singh, A. Wang, *Qualitative dynamics and inflationary attractors in loop cosmology*, *Phys. Rev. D* **98**, 066016 (2018).
- [49] S. Saini, P. Singh, *Von Neumann stability of modified loop quantum cosmologies*, *Class. Quantum Grav.* **36** (2019) 105010 [arXiv:1901.01279].
- [50] B.F. Li, P. Singh, A. Wang, *Towards cosmological dynamics from loop quantum gravity*, *Phys. Rev. D* **97**, 084029 (2018) [arXiv:1801.07313].
- [51] M. Assanioussi, A. Dapor, K. Liegener and T. Pawowski, *Emergent de Sitter epoch of the Loop Quantum Cosmos: a detailed analysis*, *Phys. Rev. D* **100**, no. 8, 084003 (2019).
- [52] K. Liegener and P. Singh, *Some physical implications of regularization ambiguities in $SU(2)$ gauge-invariant loop quantum cosmology*, (To appear in *Phys. Rev. D*) arXiv:1908.07543 [gr-qc].
- [53] D. Langlois, *Hamiltonian formalism and gauge invariance for linear perturbations in inflation*, *Class. Quant. Grav.* **11**, 389 (1994).
- [54] I. Agullo, *Primordial power spectrum from the Dapor-Liegener model of loop quantum cosmology*, *Gen. Rel. Grav.* **50** (2018) 91.
- [55] P. Diener, B. Gupt, M. Megevand, and P. Singh, *LQC with cyclic model potentials*, to appear (2020).
- [56] W. Kamiski, M. Kolanowski and J. Lewandowski, "Dressed metric predictions revisited," arXiv:1912.02556 [gr-qc]
- [57] K. Giesel, A. Herzog and P. Singh, *Gauge invariant variables for cosmological perturbation theory using geometrical clocks*, *Class. Quant. Grav.* **35**, 155012 (2018).
- [58] E. Komatsu et al, *Seven-year Wilkinson microwave anisotropy probe (WMAP) observations: cosmological interpretation*, *Astrophys. J. Suppl.* **192**(2), 18 (2011) [arXiv:1001.4538].
- [59] B. Bolliet, J. Grain, C. Stahl, L. Linsefors, and A. Barrau, *Comparison of primordial tensor power spectra from the deformed algebra and dressed metric approaches in loop quantum cosmology*, *Phys. Rev. D* **91**, 084035 (2015).